

New Algebraic Formulation of Density Functional Calculation

Sohrab Ismail-Beigi[†] and T.A. Arias[‡]

[†] Department of Physics, Massachusetts Institute of Technology,
Cambridge, Massachusetts 02139

[‡] Laboratory of Atomic and Solid State Physics, Cornell University,
Ithaca, New York 14853

and

[‡] Research Laboratory of Electronics, Massachusetts Institute of Technology,
Cambridge, Massachusetts 02139

Suggested PACS codes: 71.15.-m, 71.15.Ap, 71.15.Fv, 71.15.Hx.

Keywords: density-functional theory, ab initio calculations, electronic structure methods, electronic structure calculations, high performance computing, parallel computing, computer languages

In press: Comp. Phys. Comm., vol. **128**, pp. 1-45 (June 2000).

Abstract

This article addresses a fundamental problem faced by the community employing single-particle *ab initio* methods: the lack of an effective formalism for the rapid exploration and exchange of new methods. To rectify this, we introduce a new, basis-set independent, matrix-based formulation of generalized density functional theories which reduces the development, implementation, and dissemination of new techniques to the derivation and transcription of a few lines of algebra. This new framework enables us to concisely demystify the inner workings of fully functional, highly efficient modern *ab initio* codes and to give complete instructions for their construction for calculations employing arbitrary basis sets. Within this framework, we also discuss in full detail a variety of leading-edge techniques, minimization algorithms, and highly efficient computational kernels for use with scalar as well as shared and distributed-memory supercomputer architectures.

Contents

1	Introduction	3
2	Overview	6
3	Lagrangian formalism	7
4	Basis-set independent matrix formulation	9
4.1	Basis-dependent operators	10
4.2	Identities satisfied by the basis-dependent operators	11
4.3	Basis-independent expression for the Lagrangian	12
4.3.1	Kinetic energy	13
4.3.2	Electron-ion interaction	13
4.3.3	Exchange-correlation energy	13
4.3.4	Hartree self-energy	13
4.3.5	Electron-Hartree interaction	14
4.3.6	Complete Lagrangian	14
4.4	Orthonormality constraints	14
4.5	Derivatives of the Lagrangian	15
4.5.1	Derivative with respect to the electronic states	15
4.5.2	Derivative with respect to the Hartree field	16
4.5.3	Derivative with respect to subspace rotations	17
4.6	Kohn-Sham and Poisson equations	18
4.7	Expressions for Lagrangian and derivatives: summary	19
5	DFT++ specification for various <i>ab initio</i> techniques	19
5.1	Local spin-density approximation (LSDA)	20
5.2	Self-interaction correction	21
5.3	Band-structure and fixed Hamiltonian calculations	23
5.4	Unoccupied states	23
5.5	Variational density-functional perturbation theory	24
6	Minimization algorithms	26
6.1	Semiconducting and insulating systems	27
6.2	Metallic and high-temperature systems	29
7	Implementation, optimization, and parallelization	31
7.1	Object-oriented implementation in C++	32
7.2	Scalings for dominant DFT++ operations	33
7.3	Optimization of computational kernels	35
7.4	Parallelization	39
7.4.1	Shared-memory (SMP) architectures	40
7.4.2	Distributed-memory (DMP) architectures	44
8	Acknowledgements	47

A	Plane-wave implementation of the basis-dependent operators	48
B	Non-local potentials	49
C	Multiple k-points	51
D	Complete LDA code with k-points and non-local potentials	53
E	The Q operator	53

List of Tables

1	FLOP count of dominant DFT++ operations	35
---	---	----

List of Figures

1	Overview of DFT++ formalism	5
2	LDA energy routine (DFT++ formalism)	27
3	Steepest descent algorithm	28
4	Quadratic line minimizer	28
5	Preconditioned conjugate-gradient algorithm	29
6	Effect of subspace rotation on convergence	31
7	LDA energy routine (C++ implementation)	34
8	Blocked matrix multiplication	37
9	Matrix-multiplication FLOP rates (single processor)	39
10	Scaling for SMP parallelization	42
11	Amdahl's analysis of SMP scaling	43
12	Transposition of distributed matrices	44
13	Scaling of DMP parallelization	45
14	Amdahl's analysis of DMP scaling	46

1 Introduction

This work gives a self-contained description of how to build a highly flexible, portable density-functional production code which attains significant fractions of peak performance on scalar cached architectures, shared-memory processors (SMP), and distributed-memory processors (DMP). More importantly, however, this work introduces a new formalism, DFT++, for the development, implementation, and dissemination of new *ab initio* generalized functional theoretic techniques among researchers. The most well-known and widely used generalized functional theory (GFT) is density-functional theory, where the energy of the system is parametrized as a functional of the electron density. Although the formalism presented here is applicable to other single-particle GFTs, such as self-interaction correction or Hartree-Fock theory, for concreteness we concentrate primarily on density functional theory (DFT).

This formalism is of particular interest to those on the forefront of exploring new *ab initio* techniques and novel applications of such in the physical sciences. It allows practitioners to quickly introduce new physics and techniques without expenditure of significant effort in debugging and optimizing or in developing entirely new software packages. It does so by providing a new, compact, and explicit matrix-based language for expressing GFT calculations, which allows new codes to be “derived” through straightforward formal manipulations. It also provides a high degree of modularity, a great aid in maintaining high computational performance.

This language may be thought of as being for GFT what the Dirac notation is for quantum mechanics: a fully explicit notation free of burdensome details which permits the ready performance of complex manipulations with focus on physical content. Direct application of the Dirac notation to GFT is particularly cumbersome because in single-particle theories, the quantum state of the system is not represented by a single ket but rather a collection of kets, necessitating a great deal of indexing. Previous attempts to work with the Dirac notation while eliminating this indexing have included construction of column vectors whose entries were kets [1] but such constructions have proved awkward because, ultimately, kets are members of an abstract Hilbert space and are not the fundamental objects of an actual calculation.

The foundation of the new DFT++ formalism is the observation that all the necessary computations in an *ab initio* calculation can be expressed explicitly as standard linear-algebraic operations upon the actual computational representation of the quantum state without reference to complicated indexing or to the underlying basis set. With traditional approaches, differentiating the energy functional, which is required for self-consistent solution for the single-particle orbitals, is a frequent source of difficulty. Issues arise such as the distinction between wave functions and their duals, covariant versus contravariant quantities, establishing a consistent set of normalization conventions, and translation from continuum functional derivatives to their discrete computational representations. However, by expressing the energy explicitly in our formalism, all these difficulties are automatically avoided by straightforward differentiation of a well-defined linear-algebraic expression.

This new formalism allows not only for ease of formal manipulations but also for direct transcription of the resulting expressions into software, i.e. literal typing of physical expressions in their matrix form into lines of computer code. Literal transcription of operations such as matrix addition and multiplication is possible through the use of any of the modern, high-level computer languages which allows for the definition of new object types (e.g. vectors and matrices) *and* the action of the standard operators such as “+”, “-”, or “*” upon them. Once the basic operators have been implemented, the task of developing and debugging is simplified to checking the formulae which have been entered into the software. This allows the researcher to modify or extend the software and explore entirely new physical ideas rapidly. Finally, a very important practical benefit of using matrix operations wherever possible is that the theory of attaining peak performance on modern computers is well developed for matrix-matrix multiplication.

The high level of modularity which naturally emerges within the DFT++ formalism compartmentalizes and isolates from one another the primary areas of research in electronic structure calculation: (i) derivation of new physical approaches, (ii) development of effective numerical techniques for reaching self-consistency, and (iii) optimization and parallelization of the underlying computational kernels. This compartmentalization brings the significant

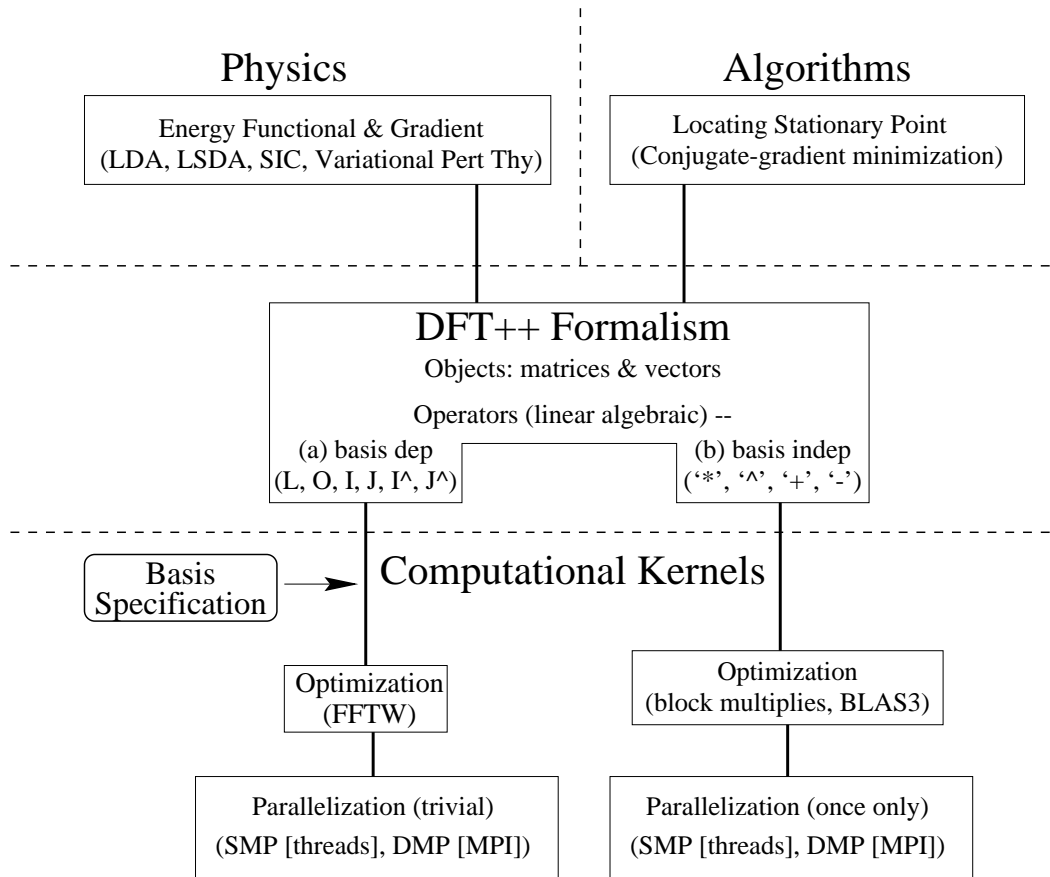


Figure 1: Overview of DFT++ formalism

advantage that researchers with specialized skills can explore effectively the areas which pertain to them, without concerning themselves with the areas with which they are less familiar.

A few anecdotes from our own experience serve to illustrate the efficacy of this approach. The extension of our production software to include electron spin through the local spin-density approximation (LSDA) required a student with no prior familiarity with our software only one-half week to gain that familiarity, three days to redefine the software objects to include spin, and less than one day to implement and debug the new physics. The time it took another student to develop, implement, explore, and fine-tune the new numerical technique of Section 6.2 was less than a week. Finally, our experience with parallelization and optimization has been similarly successful. To parallelize our software for use with an SMP (using threads) required a student starting with no prior knowledge of parallelization two weeks to develop a code which *sustains* an average per processor FLOP rate of 80% of the processor clock speed. (See Section 7.4.1 for details.) Finally, for massively parallel applications, the development of an efficient DMP code (based on MPI), a task which often requires a year or more, required two students working together approximately two months to complete.

2 Overview

Figure 1 both illustrates the interconnections among the primary areas of active research in modern electronic structure calculations and serves as a road-map for the content of this article. The figure emphasizes how the DFT++ formalism forms an effective central bridge connecting these areas.

Reduction to practice of new physical approaches generally requires expressions for an energy functional and the derivatives of that functional, as indicated in the upper-left portion of the figure. Our discussion begins in Section 3 with an exposition of the mathematical framework which we employ throughout this work, a Lagrangian formulation of generalized density functional theories. In Section 4 we introduce our matrix-based formalism using density-functional theory (DFT) within the local-density approximation (LDA) [2] as a case study, deriving the requisite expressions for the energy functional and its gradient.

In Section 5, we go on to consider several examples of other functionals for physical calculations, including the local spin-density approximation (LSDA), self-interaction correction (SIC), density-functional variational perturbation theory, and band-structure calculations. We derive the requisite expressions for the corresponding functionals and their derivatives in the space of a few pages and thereby show the power and compactness of our formulation for the treatment of a wide range of single-particle quantum mechanical problems.

As mentioned in the introduction, our matrix-based formalism allows the relevant formulae to be literally typed into the computer. Because these formulae are self-contained, we can make, as illustrated in the upper-right portion of the figure, a clear distinction between the expression of the physics itself and the algorithms which search for the stationary point of the energy functional to achieve self-consistency. For concreteness, in Section 6 we provide full specification for both a preconditioned conjugate-gradient minimization algorithm and a new algorithm for accelerating convergence when working with metallic systems.

Due to our matrix-based formulation, the expressions for the objective function and its derivatives are built from linear-algebraic operations involving matrices. As the lower portion of Figure 1 illustrates, the DFT++ formalism clearly isolates the software which contains the actual computational kernels. These kernels therefore may be optimized and parallelized independently from all other considerations.

Section 7 describes these computational considerations in detail. In Section 7.1 we discuss the use of object-oriented languages for linking the underlying computational kernels with higher level physical expressions. Section 7.2 discusses the scaling with physical system size of the burden for the most time consuming computational kernels. There are in fact two distinct types of computational kernels, both of which appear in the lower portion of the figure.

The first type are kernels which implement those few operators in our formalism that depend on the choice of basis set (L , \mathcal{O} , \mathcal{I} , \mathcal{J} , \mathcal{I}^\dagger , \mathcal{J}^\dagger , defined in Section 4.1). These kernels represent the only entrance of basis-set details into the overall framework. (Appendix A provides the requisite details for plane-wave calculations.) This allows for coding of new physics and algorithms without reference to the basis and for a single higher-level code to be used with “plug-ins” for a variety of different basis sets. The application of the basis-dependent operators can be optimized as discussed in Section 7.3 by calling standard packages such as FFTW [3]. Parallelization for the basis-dependent operators is trivial because they act in parallel on all of the electronic wave functions at once. Section 7.4

discusses such parallelization for SMP and DMP architectures.

Finally, the second class of kernels are basic linear-algebraic operations (e.g. matrix multiplication '*', addition '+', subtraction '-', and Hermitian-conjugated multiplication '^') which do not in any way depend on the basis set used for the calculation. As such, the work of optimization and parallelization for these kernels need only be performed once. Section 7.3 presents the two strategies we employ for these optimizations: blocking of matrix multiplication and calling optimized linear-algebra packages such as BLAS3. Parallelization of these operations is not trivial because data-sharing or communication is required between processors. We detail high performance strategies for dealing with this issue in Sections 7.4 for both SMP and DMP architectures.

3 Lagrangian formalism

The traditional equations of density-functional theory are the Kohn-Sham equations [2] for a set of effective single-particle electronic states $\{\psi_i(r)\}$. Below, when we refer to “electrons”, we are in fact always referring to these effective electronic degrees of freedom. The electrostatic or Hartree field $\phi(r)$ caused by the electrons is traditionally found from solving the Poisson equation with the electron density derived from these wave functions as the source term. The ground-state energy of the system is then found by minimizing the traditional energy functional, which ensures the self-consistent solution of the Kohn-Sham equations. A great advantage of this variational principle is that first-order errors in the wave functions lead to only second order errors in the energy. However, although not frequently emphasized, errors in solving the Poisson equation due to the incompleteness of the basis set used in a calculation may produce a non-variational (i.e. first-order) error in the energy.

We now consider a new variational principle which ultimately leads to identical results for complete basis sets, but which places $\{\psi_i\}$ and ϕ on an equal footing and has several advantages in practice. The central quantity in this principle is the Lagrangian \mathcal{L}_{LDA} introduced in [4], which within the local-density approximation (LDA), is

$$\begin{aligned} \mathcal{L}_{LDA}(\{\psi_i(r)\}, \phi(r)) = & -\frac{1}{2} \sum_i f_i \int d^3r \psi_i^*(r) \nabla^2 \psi_i(r) \\ & + \int d^3r V_{ion}(r) n(r) + \int d^3r \epsilon_{xc}(n(r)) n(r) \\ & - \int d^3r \phi(r) (n(r) - n_0) - \frac{1}{8\pi} \int d^3r \|\vec{\nabla}\phi(r)\|^2, \end{aligned} \quad (1)$$

where the electron density $n(r)$ is defined in terms of the electronic states and the Fermi-Dirac fillings f_i as

$$n(r) = \sum_i f_i \|\psi_i(r)\|^2. \quad (2)$$

Here and throughout this article we work in atomic units and therefore have set $\hbar = m_e = e = 1$, where m_e is the electron mass and e is the charge of the proton. Finally, the Kohn-Sham electronic states $\{\psi_i\}$ must satisfy the orthonormality constraints

$$\int d^3r \psi_i^*(r) \psi_j(r) = \delta_{ij}. \quad (3)$$

Above, $\epsilon_{xc}(n)$ is the exchange-correlation energy per electron of a uniform electron gas with electron density n , and $V_{ion}(r)$ is the potential each electron feels due to the ions. The constant n_0 is used in calculations in periodic systems as a uniform positive background that neutralizes the electronic charge density. The effect of this background on the total energy is properly compensated when the Ewald summation is used to compute the interionic interactions.

The following equations, subject to the constraints of Eq. (3), specify the stationary point of \mathcal{L}_{LDA} ,

$$\frac{1}{f_i} \frac{\delta \mathcal{L}_{LDA}}{\delta \psi_i^*(r)} = 0 = \left[-\frac{1}{2} \nabla^2 + V_{ion}(r) - \phi(r) + V_{xc}(r) \right] \psi_i(r) - \epsilon_i \psi_i(r), \quad (4)$$

$$\frac{\delta \mathcal{L}_{LDA}}{\delta \phi(r)} = 0 = -(n(r) - n_0) + \frac{1}{4\pi} \nabla^2 \phi(r). \quad (5)$$

These are seen to be the standard Kohn-Sham eigenvalue equations for $\psi_i(r)$ and the Poisson equation for the Hartree potential $\phi(r)$ where the negative sign in the second equation properly accounts for the negative charge of the electrons.

The behavior of \mathcal{L}_{LDA} is in fact quite similar to that of the traditional LDA energy functional,

$$\begin{aligned} E_{LDA}(\{\psi_i(r)\}) &= -\frac{1}{2} \sum_i f_i \int d^3r \psi_i^*(r) \nabla^2 \psi_i(r) + \int d^3r V_{ion}(r) n(r) \\ &+ \int d^3r \epsilon_{xc}(n(r)) n(r) + \frac{1}{2} \int d^3r \int d^3r' \frac{n(r)n(r')}{\|r - r'\|}. \end{aligned} \quad (6)$$

First, as shown in [5], evaluation of $\mathcal{L}_{LDA}(\{\psi_i(r)\}, \tilde{\phi}(r))$, where $\tilde{\phi}$ is the solution of the Poisson equation, recovers the value of the traditional energy functional. Moreover, the derivatives of \mathcal{L}_{LDA} and E_{LDA} are also equal at $\tilde{\phi}$. This result follows by considering a variation of the equality $E_{LDA}(\{\psi_i(r)\}) = \mathcal{L}_{LDA}(\{\psi_i(r)\}, \tilde{\phi}(r))$, which expands into

$$\begin{aligned} \sum_i \int d^3r \left(\frac{\delta E_{LDA}}{\delta \psi_i(r)} \delta \psi_i(r) + \frac{\delta E_{LDA}}{\delta \psi_i^*(r)} \delta \psi_i^*(r) \right) &= \sum_i \int d^3r \left(\frac{\delta \mathcal{L}_{LDA}}{\delta \psi_i(r)} \delta \psi_i(r) + \frac{\delta \mathcal{L}_{LDA}}{\delta \psi_i^*(r)} \delta \psi_i^*(r) \right) \\ &+ \int d^3r \frac{\delta \mathcal{L}_{LDA}}{\delta \phi(r)} \delta \tilde{\phi}(r). \end{aligned}$$

Because Poisson's equation (Eq. (5)) is the condition that the functional derivative of \mathcal{L}_{LDA} with respect to ϕ vanishes, the last term on the right-hand side is zero when $\phi = \tilde{\phi}$. Therefore, the functional derivatives of E_{LDA} and \mathcal{L}_{LDA} with respect to the electronic states $\{\psi_i\}$ are equal when evaluated at $\tilde{\phi}(r)$. Finally, the critical points of \mathcal{L}_{LDA} are in one-to-one correspondence with the minima of E_{LDA} . The reason is that (i) for fixed $\{\psi_i\}$, there is a unique $\tilde{\phi}$ (up to a choice of arbitrary constant) which solves the Poisson equation because \mathcal{L}_{LDA} as a function of ϕ is a negative-definite quadratic form, and (ii) as we have just seen, at such points the derivatives with respect to $\{\psi_i\}$ of E_{LDA} and \mathcal{L}_{LDA} are identical.

One advantage of placing ϕ and $\{\psi_i\}$ on an equal footing is that now errors in the Lagrangian are second-order in the errors of both the wave functions *and* the Hartree field. Additionally, as a practical matter, one has greater flexibility in locating the stationary

point. Rather than solving for the optimal ϕ at each value of $\{\psi_i\}$, as is done in traditional DFT methods, one has the option of exploring in both $\{\psi_i\}$ and ϕ simultaneously. However, some care in doing this is needed, because the stationary points of \mathcal{L}_{LDA} are not extrema but saddle points. (Note that the first term of Eq. (1), the kinetic energy, is unbounded above, whereas the last term, the Hartree self-energy, is unbounded below.) This saddle has a particularly simple structure, and a method to exploit this is outlined in [6].

Finally, by allowing ϕ to be a free variable, we have rendered local all interactions among the fields. One great formal advantage is that the subtle mathematical issues in periodic systems arising from the long-range nature of the Coulomb interaction no longer require special treatment. For example, the choice of the neutralizing background n_0 in periodic systems is straightforward and is treated in detail in Section 4.3.5. Because of this and the aforementioned advantages, we will work in the Lagrangian framework throughout this article.

4 Basis-set independent matrix formulation

Our basis-set independent matrix formalism allows us to express the structure of any single-particle quantum theory in a compact and explicit way. In this section, we apply it to the Lagrangian of Eq. (1) which contains energetic terms and non-linear couplings that are common to all such theories.

To make progress, we first must deal with the fact that the Lagrangian is a function of continuous fields. When we perform a computation, we are forced to represent these fields in terms of expansions within a finite basis set. Denoting our basis functions as $\{b_\alpha(r)\}$, where Greek letters index basis functions, we expand the wave functions and Hartree potential in terms of expansion coefficients $C_{\alpha i}$ and ϕ_α through

$$\psi_i(r) = \sum_{\alpha} b_{\alpha}(r) C_{\alpha i} \quad , \quad \phi(r) = \sum_{\alpha} b_{\alpha}(r) \phi_{\alpha} \quad . \quad (7)$$

Typical and popular choices of basis functions are plane waves (i.e. Fourier modes) [7], finite-element functions [8], multiresolution analyses [5], or Gaussian orbitals [9]. Once a basis set has been chosen, \mathcal{L}_{LDA} becomes an explicit function of the finite set of variables $C_{\alpha i}$ and ϕ_{α} .

In addition to the basis set itself, we require a grid of points p in real space covering the simulation cell. This grid is necessary for a number of operations, such as for computing the values of the wave functions or the electron density in real-space and for computing the exchange-correlation energy density $\epsilon_{xc}(n(r))$ of Eq. (1), which is a non-algebraic function of the electron density $n(r)$ and can only be computed point by point on the real-space grid.

Our aim is to find a compact, matrix-based notation that works in the space of expansion coefficients $C_{\alpha i}$ and ϕ_{α} and is thus applicable to any calculation within any basis set. In the course of doing so, we will be able to clearly identify which parts of our formalism require information about the particular basis that is chosen and which parts are completely general and independent of this choice. In addition, when we have arrived at a matrix-based notation, it will be clear that only a few fundamental types of computational kernels are needed to perform the calculation, so that parallelization and optimization need only address themselves to these few kernels. This provides a great boon for portability, ease of programming, and extensibility to new physical scenarios.

In the discussion below, we describe our formalism only for the case of local ionic potentials. The use of non-local potentials (e.g. for the important case of pseudopotential calculations) results in only minor changes that are addressed in Appendix B. Furthermore, for periodic systems, we will be working with only a single k -point at $k = 0$, as is evident from the choice of expansion in Eq. (7). We work at $k = 0$ in order to keep the mathematical expressions as transparent as possible. The minor extensions required to accommodate non-zero and multiple k -points are straightforward and are dealt with in Appendix C.

4.1 Basis-dependent operators

In this section we describe all the operators in our formalism that depend on the basis set chosen for the calculation. We will see that there are a small number of such operations, and that we can easily separate their role from the rest of the formalism.

The first two operators involve matrix elements of the identity and the Laplacian between pairs of basis functions. Specifically, we define

$$\mathcal{O}_{\alpha,\beta} \equiv \int d^3r b_\alpha^*(r) b_\beta(r), \quad (8)$$

$$L_{\alpha,\beta} \equiv \int d^3r b_\alpha^*(r) \nabla^2 b_\beta(r). \quad (9)$$

We call these operators the overlap and Laplacian respectively. Note that for orthonormal bases, we have $\mathcal{O} = I$ where I is the identity matrix.

The integrals of the basis functions are the components of the column vector s ,

$$s_\alpha \equiv \int d^3r b_\alpha^*(r). \quad (10)$$

For periodic systems, we use the vector s to define a new operator $\bar{\mathcal{O}}$ through

$$\bar{\mathcal{O}} \equiv \mathcal{O} - \frac{ss^\dagger}{\Omega}, \quad (11)$$

where Ω is the volume of the periodic supercell. For calculations in systems without boundaries, the volume Ω is infinite so that $\mathcal{O} = \bar{\mathcal{O}}$. The chief use of $\bar{\mathcal{O}}$ is for solving the Poisson equation in periodic systems where divergences due to the long-range Coulomb interaction must be avoided. The automatic avoidance of such divergences and the proper choice of n_0 in Eq. (1) both follow directly from the nature of the Lagrangian as will be discussed in Section 4.3.5.

The next four operators involve the values of the basis functions on the points p of the real-space grid introduced above. The *forward transform* operator \mathcal{I} allows for changing representation from the space of expansion coefficients to the space of function values on the real-space grid. Specifically, given a basis function α and a grid point p , we define

$$\mathcal{I}_{p\alpha} = b_\alpha(p). \quad (12)$$

Thus the α th column of \mathcal{I} consists of the values of the α th basis function on the points of the real-space grid.

Next, it is at times necessary to find the expansion coefficients for a function given its values on the real-space grid. We denote this linear *inverse transform* by \mathcal{J} . In implementations where the number of grid points p is equal to the number of basis functions, the natural choice is to take $\mathcal{J} = \mathcal{I}^{-1}$ (e.g., plane-wave basis sets). However, this is not necessary: in some applications, one may choose to use a very dense real-space grid which has more points than the number of basis functions. Hence, we keep the formal distinction between \mathcal{J} and \mathcal{I}^{-1} . We will also require two *conjugate* transforms, which are the Hermitian conjugates \mathcal{I}^\dagger and \mathcal{J}^\dagger .

The final mathematical object that depends on the basis set involves the ionic potential $V_{ion}(r)$. We define a column vector V_{ion} whose components are the integrals

$$(V_{ion})_\alpha \equiv \int d^3r b_\alpha^*(r) V_{ion}(r), \quad (13)$$

which encodes overlaps of the ionic potential with the basis functions. We will use V_{ion} when evaluating the electron-ion interaction energy in Section 4.3.2.

4.2 Identities satisfied by the basis-dependent operators

Although the operators \mathcal{O} , $\bar{\mathcal{O}}$, L , \mathcal{I} , \mathcal{J} , \mathcal{I}^\dagger , and \mathcal{J}^\dagger depend on the choice of basis, they satisfy various identities which will prove important below. In addition to their formal properties, these identities allow for verification of the implementation of these operators.

The most important identity involves the constant function. To represent the constant function on the grid, we define the column vector $\mathbf{1}$ as having the value of unity on each grid point p : $\mathbf{1}_p = 1$. Many basis sets can represent this function exactly (e.g. plane waves or finite-element sets). For such bases, for all points r in the simulation cell, we must have the identity

$$\sum_\alpha (\mathcal{J}\mathbf{1})_\alpha b_\alpha(r) = 1. \quad (14)$$

Evaluating this identity on the real-space grid yields

$$\mathcal{I}\mathcal{J}\mathbf{1} = \mathbf{1}. \quad (15)$$

For basis sets that can not represent the constant function exactly, the identity of Eq. (15) and the ones below should hold approximately in the regions described by the basis.

According to Eq. (14), the vector $\mathcal{J}\mathbf{1}$ specifies the coefficients of the expansion of the constant function. Using the integrals s of Eq. (10), we can see that

$$\begin{aligned} s_\alpha &= \int d^3r b_\alpha^*(r) \\ &= \int d^3r b_\alpha^*(r) \left(\sum_\beta (\mathcal{J}\mathbf{1})_\beta b_\beta(r) \right) \\ &= (\mathcal{O}\mathcal{J}\mathbf{1})_\alpha. \end{aligned}$$

Thus we have that $s = \mathcal{O}\mathcal{J}\mathbf{1}$. We can also derive the normalization condition

$$s^\dagger \mathcal{J}\mathbf{1} = \int d^3r \sum_\alpha b_\alpha(r) (\mathcal{J}\mathbf{1})_\alpha = \int d^3r 1 = \Omega, \quad (16)$$

where Ω is the volume in which the calculation is performed.

When solving Poisson's equation for the electrostatic potential (Eq. (5)), we must take special care regarding the null space of the Laplacian operator L , which is the space of constant functions. Integrating the identity $\nabla^2 1 = 0$ against the complex conjugate of each basis function yields

$$L\mathcal{J}1 = 0. \quad (17)$$

We use this identity when dealing with the Poisson equation in periodic systems to avoid divergences due to the long-range nature of the Coulomb interaction.

4.3 Basis-independent expression for the Lagrangian

We now use the above operators to express the Lagrangian of Eq. (1) in a matrix-based, basis-independent manner. We begin by introducing two operators, “diag” and “Diag”. The operator *diag* converts a square matrix M into a column vector containing the diagonal elements of the matrix. The operator *Diag* converts a vector v into a diagonal matrix with the components of v on its diagonal. In terms of components, we have that

$$(\text{diag } M)_\alpha = M_{\alpha\alpha} \quad , \quad (\text{Diag } v)_{\alpha\beta} = v_\alpha \delta_{\alpha\beta} \quad , \quad (18)$$

where δ is the Kronecker delta. Thus, *diag* *Diag* $v = v$ for any vector v whereas *Diag* *diag* $M = M$ if and only if M is a diagonal matrix. Two useful identities involving these operators are

$$(\text{diag } M)^\dagger v = \text{Tr}(M^\dagger \text{Diag } v) \quad , \quad v^\dagger (\text{diag } M) = \text{Tr}((\text{Diag } v)^\dagger M) \quad , \quad (19)$$

where \dagger indicates Hermitian or complex-conjugated transposition.

Next, if we regard the expansion coefficients $C_{\alpha i}$ as a matrix whose i th column contains the expansion coefficients of the i th wave function (Eq. (7)), and we also define the diagonal matrix of Fermi fillings $F_{ij} = f_i \delta_{ij}$, it is easy to see that

$$P = CFC^\dagger \quad (20)$$

is the representation of the single-particle density matrix in the space of basis functions.

Before considering the Lagrangian itself, we will also need expressions for the electron density $n(r)$ which appears in most of the terms of the Lagrangian of Eq. (1). We define a vector n whose components are the values of the electron density on the points p of the real-space grid. Specifically,

$$\begin{aligned} n_p \equiv n(p) &= \sum_i f_i \|\psi_i(p)\|^2 = \sum_i f_i \|(\mathcal{I}C)_{pi}\|^2 \\ &= \sum_i (\mathcal{I}C)_{pi}^* f_i (\mathcal{I}C)_{pi} = \left((\mathcal{I}C)F(\mathcal{I}C)^\dagger \right)_{pp} \quad , \end{aligned}$$

whence we arrive at the identity defining the vector n

$$n = \text{diag}(\mathcal{I}P\mathcal{I}^\dagger) \quad . \quad (21)$$

Given the values of the electron density on the real-space grid, we use the inverse transform \mathcal{J} to find the expansion coefficients of $n(r)$ in terms of the basis functions. This vector of coefficients is just $\mathcal{J}n$.

Armed with these few tools, we now proceed to write the various energetic terms of the Lagrangian in the matrix language developed above.

4.3.1 Kinetic energy

The kinetic energy T can be transformed into the matrix language by using the expansion coefficients C of Eq. (7) and by using the definition of the Laplacian L of Eq. (9):

$$\begin{aligned} T &\equiv -\frac{1}{2} \sum_i f_i \int d^3r \psi_i^*(r) \nabla^2 \psi_i(r) = -\frac{1}{2} \sum_i f_i \sum_{\alpha,\beta} C_{\alpha i}^* L_{\alpha\beta} C_{\beta i} \\ &= -\frac{1}{2} \text{Tr} (FC^\dagger LC) = -\frac{1}{2} \text{Tr} (LP) , \end{aligned} \quad (22)$$

where the last two equivalent expressions are related by the cyclic property of the trace. Thus, we are able to write the kinetic energy explicitly as a function of the density matrix P of Eq. (20).

4.3.2 Electron-ion interaction

Since the electron density $n(r)$ is real, we may write the electron-ion interaction as

$$\begin{aligned} E_{e-i} &\equiv \int d^3r n^*(r) V_{ion}(r) = \sum_{\alpha} \int d^3r (\mathcal{J}n)_{\alpha}^* b_{\alpha}^*(r) V_{ion}(r) \\ &= (\mathcal{J}n)^\dagger V_{ion} = \text{Tr} \left(\mathcal{I}^\dagger \left[\text{Diag } \mathcal{J}^\dagger V_{ion} \right] \mathcal{I}P \right) , \end{aligned} \quad (23)$$

where we have used the definition of V_{ion} from Eq. (13) and have used Eqs. (21) and (19) to rewrite this interaction in terms of P .

4.3.3 Exchange-correlation energy

Given the vector n of electron-density values on the grid, we can evaluate the exchange-correlation energy per particle at each grid point p through $\epsilon_{xc}(n(p))$. We collect these values into a vector $\epsilon_{xc}(n)$. We then inverse transform this vector and the electron density vector, and we use the overlap operator to arrive at

$$\begin{aligned} E_{xc} &\equiv \int d^3r n^*(r) \epsilon_{xc}(n(r)) \\ &= (\mathcal{J}n)^\dagger \mathcal{O}(\mathcal{J}\epsilon_{xc}(n)) = \text{Tr} \left(\mathcal{I}^\dagger \left[\text{Diag } \mathcal{J}^\dagger \mathcal{O} \mathcal{J} \epsilon_{xc}(n) \right] \mathcal{I}P \right) , \end{aligned} \quad (24)$$

where we again have conjugated the electron density for ease of formal manipulations. The derivation of the final expression in terms of P uses Eq. (21).

4.3.4 Hartree self-energy

The self-energy of the Hartree field can be written as

$$E_{H-H} \equiv -\frac{1}{8\pi} \int d^3r \|\vec{\nabla} \phi(r)\|^2 = \frac{1}{8\pi} \int d^3r \phi^*(r) \nabla^2 \phi(r) = \frac{1}{8\pi} \phi^\dagger L \phi , \quad (25)$$

where we have first integrated by parts and then substituted the expansion coefficients ϕ of Eq. (7). The complex conjugation of the real-valued function $\phi(r)$ allows for the simplicity of the final expression.

4.3.5 Electron-Hartree interaction

The interaction of the electron density $n(r)$ and Hartree potential $\phi(r)$ can be written as

$$E_{e-H} \equiv - \int d^3r (n(r) - n_0)^* \phi(r) = - [\mathcal{J}(n - n_0 \mathbf{1})]^\dagger \mathcal{O} \phi. \quad (26)$$

The proper choice of n_0 for periodic systems can be found by noting that the Hartree self-energy E_{H-H} of Eq. (25) has no dependence on the projection of ϕ onto the null space of L which, as we saw in Section 4.2, lies along the vector $\mathcal{J}\mathbf{1}$. Thus, for the Lagrangian of Eq. (1) to have a saddle-point, there can be no coupling of $n(r) - n_0$ with the projection of ϕ along $\mathcal{J}\mathbf{1}$. That is, we must have $[\mathcal{J}(n - n_0 \mathbf{1})]^\dagger \mathcal{O} \cdot \mathcal{J}\mathbf{1} = 0$. The identities of Section 4.2 then lead to the choice $n_0 = (\mathcal{J}n)^\dagger s / \Omega$. Our final expression for E_{e-H} is thus given by

$$E_{e-H} = -(\mathcal{J}n)^\dagger \left(\mathcal{O} - \frac{ss^\dagger}{\Omega} \right) \phi = -(\mathcal{J}n)^\dagger \bar{\mathcal{O}} \phi = -\text{Tr} \left(\mathcal{I}^\dagger \left[\text{Diag } \mathcal{J}^\dagger \bar{\mathcal{O}} \phi \right] \mathcal{I} P \right). \quad (27)$$

4.3.6 Complete Lagrangian

Summing all the contributions above, we arrive at two equivalent expressions for the Lagrangian \mathcal{L}_{LDA} ,

$$\mathcal{L}_{LDA} = -\frac{1}{2} \text{Tr} (FC^\dagger LC) + (\mathcal{J}n)^\dagger [V_{ion} + \mathcal{O} \mathcal{J} \epsilon_{xc}(n) - \bar{\mathcal{O}} \phi] + \frac{1}{8\pi} \phi^\dagger L \phi \quad (28)$$

$$\begin{aligned} &= -\frac{1}{2} \text{Tr} (LP) + \frac{1}{8\pi} \phi^\dagger L \phi \\ &\quad + \text{Tr} \left(\mathcal{I}^\dagger \text{Diag} \left[\mathcal{J}^\dagger V_{ion} + \mathcal{J}^\dagger \mathcal{O} \mathcal{J} \epsilon_{xc}(n) - \mathcal{J}^\dagger \bar{\mathcal{O}} \phi \right] \mathcal{I} P \right). \end{aligned} \quad (29)$$

The first, compact form is computationally efficient for evaluating the Lagrangian as a function of C and ϕ . The second form, written as a function of the density matrix P , finds its best use in the formal manipulations required to find the gradient of the Lagrangian.

4.4 Orthonormality constraints

The orthonormality constraints of Eq. (3) are equivalent to the matrix equation

$$C^\dagger \mathcal{O} C = I. \quad (30)$$

If we wish to compute gradients of the Lagrangian with respect to C in order to arrive at the Kohn-Sham equations, we must do so while always obeying these constraints.

The analytically-continued functional approach [1] deals with these constraints by introducing a set of expansion coefficients Y which are *unconstrained* and which can have any overlap U ,

$$U = Y^\dagger \mathcal{O} Y. \quad (31)$$

We also allow for the possibility of subspace rotation, which is a unitary transformation mapping the subspace of occupied states $\{\psi_i\}$ onto itself. Such a transformation is affected by a unitary matrix V , and we parameterize V as the exponential of a Hermitian matrix B through

$$V \equiv e^{iB} \quad \text{where} \quad B^\dagger = B. \quad (32)$$

The coefficients C are defined as dependent variables through the mapping

$$C = YU^{-1/2}V^\dagger, \quad (33)$$

which ensures that Eq. (30) is automatically obeyed, as is easy to verify by direct substitution. The density matrix P takes the following form in terms of Y and V ,

$$P = CFC^\dagger = YU^{-1/2}V^\dagger F V U^{-1/2}Y^\dagger. \quad (34)$$

In most cases, we simply set $V = I$. In fact, for the case of constant fillings, $F = fI$, the unitary matrix V drops out of P completely. The subspace rotations find their primary use in the study of metallic or high-temperature systems where the Fermi-Dirac fillings are not constant, and the rotations allow for greatly improved convergence rates when searching for the saddle point of the Lagrangian. This point is explained in more detail in Section 6.

4.5 Derivatives of the Lagrangian

Since the most effective modern methods that search for stationary points require knowledge of the derivative of the objective function, we will now find the derivative of the Lagrangian of Eq. (28) or (29) with respect to the variables Y and ϕ (and B if subspace rotations are used). Differentiation with respect to Y is far more complex due to the orthonormality constraints, and we begin with this immediately.

4.5.1 Derivative with respect to the electronic states

Computing the derivative of the Lagrangian with respect to Y is intricate, and we break the problem into smaller pieces by first finding the derivative with respect to the density matrix P . Once the derivative with respect to P is found, we can use the relation between P and Y (Eq. (34)) to find the derivative with respect to Y .

We begin by noting that except for the exchange-correlation energy, the entire expression of Eq. (29) is linear in the density matrix P . The exchange-correlation energy is a function of the electron density n , which, through Eq. (21), is also a function of P . Thus if we consider a differential change dP of the density matrix, the only term in $d\mathcal{L}_{LDA}$ that needs to be considered carefully is

$$\begin{aligned} n^\dagger \mathcal{J}^\dagger \mathcal{O} \mathcal{J} d[\epsilon_{xc}(n)] &= n^\dagger \mathcal{J}^\dagger \mathcal{O} \mathcal{J} [\text{Diag } \epsilon'_{xc}(n)] dn \\ &= \text{Tr} \left\{ \mathcal{I}^\dagger \text{Diag} \left([\text{Diag } \epsilon'_{xc}(n)] \mathcal{J}^\dagger \mathcal{O} \mathcal{J} n \right) \mathcal{I} dP \right\}. \end{aligned}$$

In the above derivation, we have used Eq. (21) to relate dn to dP as well as the identities of Eq. (19). The vector $\epsilon'_{xc}(n)$ is given by its values on the real-space grid points p via $(\epsilon'_{xc}(n))_p \equiv \epsilon'_{xc}(n(p))$.

We can now write the differential of the Lagrangian of Eq. (29) with respect to P as

$$\begin{aligned} d\mathcal{L}_{LDA} &= \text{Tr} \left\{ -\frac{1}{2} L dP + \mathcal{I}^\dagger \text{Diag} \left[\mathcal{J}^\dagger V_{ion} + \mathcal{J}^\dagger \mathcal{O} \mathcal{J} \epsilon_{xc}(n) \right. \right. \\ &\quad \left. \left. + [\text{Diag } \epsilon'_{xc}(n)] \mathcal{J}^\dagger \mathcal{O} \mathcal{J} n - \mathcal{J}^\dagger \bar{\mathcal{O}} \phi \right] \mathcal{I} dP \right\} \\ &\equiv \text{Tr} (H dP), \end{aligned} \quad (35)$$

where the single-particle Kohn-Sham Hamiltonian operator H is given by

$$\begin{aligned} H &= -\frac{1}{2}L + \mathcal{I}^\dagger[\text{Diag } V_{sp}]\mathcal{I}, \quad \text{where} \\ V_{sp} &= \mathcal{J}^\dagger V_{ion} + \mathcal{J}^\dagger \mathcal{O} \mathcal{J} \epsilon_{xc}(n) + [\text{Diag } \epsilon'_{xc}(n)] \mathcal{J}^\dagger \mathcal{O} \mathcal{J} n - \mathcal{J}^\dagger \bar{\mathcal{O}} \phi. \end{aligned} \quad (36)$$

The single-particle Hamiltonian is the sum of a kinetic operator and a local single-particle potential V_{sp} (a vector of numbers on the real-space grid specifying the values of the potential).

Eq. (35) has conveniently separated out the physical description of the system, the Hamiltonian H , from the variation dP which we now compute. Differentiating the relation $U^{-1/2}U^{1/2} = I$, we find that

$$d[U^{-1/2}] = -U^{-1/2}d[U^{1/2}]U^{-1/2},$$

and we use this to express the variation of the density matrix of Eq. (34) as

$$\begin{aligned} dP &= (dY)U^{-1/2}V^\dagger FVU^{-1/2}Y^\dagger + YU^{-1/2}V^\dagger FVU^{-1/2}(dY^\dagger) \\ &\quad - YU^{-1/2} \left(d[U^{1/2}]U^{-1/2}V^\dagger FV + V^\dagger FVU^{-1/2}d[U^{1/2}] \right) U^{-1/2}Y^\dagger. \end{aligned}$$

We now substitute this expression for dP into Eq. (35). We use the definition of the operator Q (Eq. (55) of Appendix E), its relation to $d[U^{1/2}]$ (Eq. (54)), and the identities which Q satisfies (Eqs. (56)). After some manipulations involving the cyclicity of the trace, we arrive at

$$\begin{aligned} d\mathcal{L}_{LDA} &= \text{Tr} \left[dY^\dagger \left(\frac{\partial \mathcal{L}_{LDA}}{\partial Y^\dagger} \right) + \left(\frac{\partial \mathcal{L}_{LDA}}{\partial Y^\dagger} \right)^\dagger dY \right], \quad \text{where} \\ \left(\frac{\partial \mathcal{L}_{LDA}}{\partial Y^\dagger} \right) &\equiv (I - \mathcal{O}CC^\dagger) HCFVU^{-1/2} + \mathcal{O}CVQ (V^\dagger[\tilde{H}, F]V), \quad \text{and} \\ \tilde{H} &\equiv C^\dagger HC, \end{aligned} \quad (37)$$

where \tilde{H} is the subspace Hamiltonian and contains matrix elements of the Hamiltonian H among the wave functions $\{\psi_i(r)\}$. Square brackets denote the commutator, $[a, b] \equiv ab - ba$. Physical interpretation of the terms in Eq. (37) is provided in Section 4.6.

Finally, since Y and Y^\dagger are not independent, we can simplify the expression for the differential of \mathcal{L}_{LDA} to

$$d\mathcal{L}_{LDA} = 2 \text{Re} \text{Tr} \left[dY^\dagger \left(\frac{\partial \mathcal{L}_{LDA}}{\partial Y^\dagger} \right) \right],$$

where Re denotes the real part of its argument.

4.5.2 Derivative with respect to the Hartree field

Since the Lagrangian in Eq. (28) is quadratic in ϕ , its derivative with respect to ϕ may be readily calculated. However, to arrive at a symmetric expression for the derivative in terms of ϕ and ϕ^\dagger , we note that the linear dependence on ϕ , given by $z \equiv (\mathcal{J}n)^\dagger \bar{\mathcal{O}}\phi$, is a real number because both $n(r)$ and $\phi(r)$ are real in Eq. (26). For convenience, we rewrite this

as $(z + z^*)/2$, which is an equivalent expression symmetric in ϕ and ϕ^\dagger . By using this, we compute the variation of \mathcal{L}_{LDA} and arrive at

$$\begin{aligned} d\mathcal{L}_{LDA} &= d\phi^\dagger \left(\frac{\partial \mathcal{L}_{LDA}}{\partial \phi^\dagger} \right) + \left(\frac{\partial \mathcal{L}_{LDA}}{\partial \phi} \right)^\dagger d\phi, \text{ where} \\ \left(\frac{\partial \mathcal{L}_{LDA}}{\partial \phi} \right) &\equiv -\frac{1}{2} \bar{\mathcal{O}} \mathcal{J} n + \frac{1}{8\pi} L\phi. \end{aligned} \quad (38)$$

Again, since ϕ and ϕ^\dagger are not independent, we can express the variation as

$$d\mathcal{L}_{LDA} = 2 \operatorname{Re} \left[d\phi^\dagger \left(\frac{\partial \mathcal{L}_{LDA}}{\partial \phi^\dagger} \right) \right].$$

4.5.3 Derivative with respect to subspace rotations

We have parameterized the unitary matrix V of Eq. (33) by the Hermitian matrix B of Eq. (32) as $V = e^{iB}$. We will now find the derivative of \mathcal{L}_{LDA} with respect to B . First, we consider the variation of \mathcal{L}_{LDA} with respect to those of V and V^\dagger by using Eq. (35) as our starting point. Using the definition of P in Eq. (34), we have that

$$\begin{aligned} d\mathcal{L}_{LDA} &= \operatorname{Tr}\{H dP\} \\ &= \operatorname{Tr}\{HYU^{-1/2}[dV^\dagger FV + V^\dagger FdV]U^{-1/2}Y^\dagger\} \\ &= \operatorname{Tr}\{\tilde{H}'[dV^\dagger FV + V^\dagger FdV]\}, \end{aligned}$$

where $\tilde{H}' = U^{-1/2}Y^\dagger H Y U^{-1/2}$. Differentiating the identity $V^\dagger V = I$ leads to $dV^\dagger = -V^\dagger dV V^\dagger$ which allows us to write

$$d\mathcal{L}_{LDA} = \operatorname{Tr}\{[\tilde{H}', F]dV V^\dagger\},$$

where again $\tilde{H} = C^\dagger H C$ is the subspace Hamiltonian.

We place the eigenvalues of B on the diagonal of a diagonal matrix β and place the eigenvectors of B in the columns of a unitary matrix Z . Thus $B = Z\beta Z^\dagger$ and $Z^\dagger Z = Z Z^\dagger = I$. We now use the result of Eq. (53) of Appendix E applied to the case $V = f(B) = e^{iB}$ to arrive at the following result relating dV to dB :

$$(Z^\dagger dV Z)_{nm} = (Z^\dagger dB Z)_{nm} \cdot \begin{cases} ie^{i\beta_n} & \text{if } m = n \\ \left[\frac{e^{i\beta_m} - e^{i\beta_n}}{\beta_m - \beta_n} \right] & \text{if } m \neq n \end{cases}.$$

Using this and the fact that $V^\dagger = Z e^{-i\beta} Z^\dagger$, we have that

$$\begin{aligned} d\mathcal{L}_{LDA} &= \operatorname{Tr}\{[\tilde{H}', F]Z(Z^\dagger dV Z)Z^\dagger V^\dagger\} \\ &= \operatorname{Tr}\{Z^\dagger[\tilde{H}', F]Z(Z^\dagger dV Z)e^{-i\beta}\} \\ &= \sum_{n,m} (Z^\dagger[\tilde{H}', F]Z)_{nm} (Z^\dagger dB Z)_{mn} \cdot \begin{cases} i & \text{if } m = n \\ \left[\frac{e^{i\beta_m} - e^{i\beta_n} - 1}{\beta_m - \beta_n} \right] & \text{if } m \neq n \end{cases}. \end{aligned}$$

We define the operator $R(A)$ acting on a general matrix A via

$$(Z^\dagger R(A)Z)_{nm} \equiv (Z^\dagger AZ)_{nm} \cdot \begin{cases} i & \text{if } m = n \\ \left[\frac{e^{i\beta_m - i\beta_n} - 1}{\beta_m - \beta_n} \right] & \text{if } m \neq n \end{cases} .$$

This allows us to write the variation of \mathcal{L}_{LDA} as

$$d\mathcal{L}_{LDA} = \text{Tr} \left\{ Z^\dagger R([\tilde{H}, F]) Z Z^\dagger dBZ \right\} = \text{Tr} \left\{ R([\tilde{H}, F]) dB \right\} ,$$

so that the derivative of \mathcal{L}_{LDA} with respect to B is

$$\frac{\partial \mathcal{L}_{LDA}}{\partial B} = R([\tilde{H}, F]) . \quad (39)$$

4.6 Kohn-Sham and Poisson equations

The Kohn-Sham and Poisson equations (Eqs. (4) and (5)) are obtained by setting the derivative of the Lagrangian with respect to Y and ϕ to zero. This results in the two equations

$$\left(\frac{\partial \mathcal{L}_{LDA}}{\partial Y^\dagger} \right) = 0 = (I - \mathcal{O}CC^\dagger) HCFVU^{-1/2} + \mathcal{O}CVQ(V^\dagger[\tilde{H}, F]V) , \quad (40)$$

$$\left(\frac{\partial \mathcal{L}_{LDA}}{\partial \phi^\dagger} \right) = 0 = -\frac{1}{2} \bar{\mathcal{O}} \mathcal{J} n + \frac{1}{8\pi} L\phi . \quad (41)$$

Eq. (40) states the stationarity of the Lagrangian with respect to variations of the wavefunction coefficients Y , and we examine it first.

We define the projection operator $\rho = \mathcal{O}CC^\dagger$ which satisfies $\rho^2 = \rho$ and which projects onto the subspace of occupied states $\{\psi_i\}$ used in the calculation. Its complement $\bar{\rho} = I - \rho$ projects onto the orthogonal subspace spanned by the unoccupied states. By multiplying Eq. (40) on the left by $\bar{\rho}$ and assuming that none of the Fermi fillings are zero, we find that

$$\bar{\rho}HC = 0 .$$

This reproduces the well known condition that at the stationary point, the Hamiltonian must map the occupied subspace onto itself.

Conversely, we can project Eq. (40) onto the occupied subspace by multiplying on the left by C^\dagger . This, combined with the fact that Q is an invertible linear operator, leads to the condition

$$[\tilde{H}, F] = 0 .$$

Given that F is a diagonal matrix, for arbitrary fillings, the subspace Hamiltonian \tilde{H} also must be diagonal: the states $\{\psi_i\}$ must be eigenstates of H with eigenvalues ϵ_i , as we have explicitly written in Eq. (4). However, if a pair of states ψ_i and ψ_j have degenerate fillings, $f_i = f_j$, then \tilde{H}_{ij} need not be zero. Converting such degenerate cases into the conventional diagonal representation requires a further unitary rotation, which, however, is not required for stationarity.

The second condition for stationarity, Eq. (41), rearranges into

$$L\phi = 4\pi \bar{\mathcal{O}} \mathcal{J} n . \quad (42)$$

We have arrived at the Poisson equation for the Hartree potential ϕ generated by the electron density n (the negative electronic charge is reflected by the positive coefficient of the right-hand side). Since we have explicitly projected out the null-space of L from the right-hand side, we may invert L and find the solution to the Poisson equation

$$\phi = 4\pi L^{-1} \bar{\mathcal{O}} \mathcal{J} n. \quad (43)$$

Finally, if we substitute the result of Eq. (43) for ϕ into our Lagrangian, we find the LDA energy functional (cf. Eq. (6)):

$$E_{LDA} = -\frac{1}{2} \text{Tr} (FC^\dagger LC) + (\mathcal{J}n)^\dagger \left[V_{ion} + \mathcal{O} \mathcal{J} \epsilon_{xc}(n) - \frac{1}{2} \bar{\mathcal{O}} (4\pi L^{-1} \bar{\mathcal{O}} \mathcal{J} n) \right]. \quad (44)$$

4.7 Expressions for Lagrangian and derivatives: summary

We now collect the expressions for the LDA Lagrangian and its derivatives in one place. As we will see in Section 7, formulae in the DFT++ notation translate directly into lines of computer code, so that we will also be specifying the computational implementation of the Lagrangian. In addition, given the Lagrangian and its derivatives, we can apply any suitable algorithm to find the stationary point (Section 6).

The key expressions are

$$\begin{aligned} \mathcal{L}_{LDA}(Y, \phi, B) &= -\frac{1}{2} \text{Tr} (FC^\dagger LC) + (\mathcal{J}n)^\dagger \left[V_{ion} + \mathcal{O} \mathcal{J} \epsilon_{xc}(n) - \bar{\mathcal{O}} \phi \right] + \frac{1}{8\pi} \phi^\dagger L \phi, \\ \frac{\partial \mathcal{L}_{LDA}}{\partial Y^\dagger} &= (I - \mathcal{O} C C^\dagger) H C F V U^{-1/2} + \mathcal{O} C V Q (V^\dagger [\tilde{H}, F] V), \\ \frac{\partial \mathcal{L}_{LDA}}{\partial \phi^\dagger} &= -\frac{1}{2} \bar{\mathcal{O}} \mathcal{J} n + \frac{1}{8\pi} L \phi, \quad \frac{\partial \mathcal{L}_{LDA}}{\partial B} = R([\tilde{H}, F]), \\ H &= -\frac{1}{2} L + \mathcal{I}^\dagger [\text{Diag } V_{sp}] \mathcal{I}, \quad \tilde{H} = C^\dagger H C. \end{aligned}$$

As discussed in Section 3, the value of \mathcal{L}_{LDA} and its Y and B derivatives are equal to the value and respective derivatives of the energy E_{LDA} of Eq. (44) when we evaluate the Lagrangian-based quantities at the solution of the Poisson equation. Therefore, the above expressions can also be used to find the derivatives of E_{LDA} , a fact that we will exploit in Section 6.

5 DFT++ specification for various *ab initio* techniques

In the previous section, we presented a detailed derivation of the expression for the LDA Lagrangian and its derivatives in the DFT++ formalism. We believe that the community of physicists and chemists using this and other general-functional methods should use this formalism for the communication of new energy functionals and comparisons among them.

From a physicist's or chemist's viewpoint, which we adopt in this section, linear algebra and matrices are the settings in which quantum mechanical computations must be

performed. Therefore, they are the fundamental objects in the new formalism. This is in contrast with the Dirac notation, which while an excellent conceptual tool for studying quantum problems, can never be used to carry out an actual calculation: matrix elements of bras and kets must first be found before an actual computation can proceed.

Once an expression for an energy functional is found, its derivative is found by straightforwardly differentiating it with respect to the matrices of independent variables. Armed with expressions for the functional and its derivative, the methods discussed in Section 6 can then be applied to achieve self-consistency.

In this spirit, we now present a few examples of energy functionals. Some are extensions of the LDA, while others are similar to the LDA only in that they involve the study of single-particle systems. In all cases, our aim will be to show how quickly and easily we can find the requisite expressions for the appropriate functional and its derivative.

5.1 Local spin-density approximation (LSDA)

The most straightforward generalization of the LDA approximation is to allow for spin-up and spin-down electrons to have different wave functions but to still treat exchange-correlation energies in a local approximation. Specifically, the exchange-correlation energy per particle at position r is now a function of both the spin-up and spin-down electron densities, $n_\uparrow(r)$ and $n_\downarrow(r)$, and the total LSDA exchange-correlation energy is given by

$$E_{xc} = \int d^3r n(r) \epsilon_{xc}(n_\uparrow(r), n_\downarrow(r)) ,$$

where $n(r) = n_\uparrow(r) + n_\downarrow(r)$ is the total electron density. The LSDA has been found to show substantial improvements over the LDA for atomic and molecular properties [10, 11] since the spin of the electrons is explicitly dealt with.

The changes required in the expressions of the Lagrangian and its derivatives in order to incorporate the LSDA are straightforward and easy to implement. We label spin states by σ , which can take the value \uparrow or \downarrow . We have spin-dependent expansion coefficient matrices C_σ for the wave functions (cf. Eq. (7)). Each spin channel has its own fillings F_σ and density matrix P_σ ,

$$P_\sigma = C_\sigma F_\sigma C_\sigma^\dagger .$$

The electron densities n_σ and the total electron density n are given by (cf. Eq. (21))

$$n_\sigma = \text{diag}(\mathcal{I}P_\sigma\mathcal{I}^\dagger) \quad \text{and} \quad n = \sum_\sigma n_\sigma .$$

The LSDA Lagrangian is given by

$$\mathcal{L}_{LSDA}(C_\uparrow, C_\downarrow, \phi) = -\frac{1}{2} \sum_\sigma \text{Tr} (F_\sigma C_\sigma^\dagger L C_\sigma) + (\mathcal{J}n)^\dagger [V_{ion} + \mathcal{O}\mathcal{J}\epsilon_{xc}(n_\uparrow, n_\downarrow) - \bar{\mathcal{O}}\phi] + \frac{1}{8\pi} \phi^\dagger L \phi .$$

The orthonormal expansion coefficients C_σ are found from unconstrained variables Y_σ via

$$C_\sigma = Y_\sigma U_\sigma^{-1/2} , \quad \text{where} \quad U_\sigma = Y_\sigma^\dagger \mathcal{O} Y_\sigma ,$$

where, for simplicity, we have set subspace rotations to unity, $V_\sigma = I$. Finding the derivatives of the Lagrangian with respect to the coefficients Y_σ follows the analysis of Section 4.5.1. Each spin channel has a single-particle Hamiltonian H_σ given by

$$H_\sigma = -\frac{1}{2}L + \mathcal{I}^\dagger [\text{Diag } V_\sigma] \mathcal{I}, \text{ where}$$

$$V_\sigma = \mathcal{J}^\dagger V_{ion} + \mathcal{J}^\dagger \mathcal{O} \mathcal{J} \epsilon_{xc}(n_\uparrow, n_\downarrow) + \text{Diag} \left[\frac{\partial \epsilon_{xc}(n_\uparrow, n_\downarrow)}{\partial n_\sigma} \right] \mathcal{J}^\dagger \mathcal{O} \mathcal{J} n - \mathcal{J}^\dagger \bar{\mathcal{O}} \phi.$$

The derivative of the Lagrangian with respect to Y_σ (cf. Eq. (37)) is given by

$$\left(\frac{\partial \mathcal{L}_{LSDA}}{\partial Y_\sigma^\dagger} \right) = (I - \mathcal{O} C_\sigma C_\sigma^\dagger) H_\sigma C_\sigma F_\sigma U_\sigma^{-1/2} + \mathcal{O} C_\sigma Q([\tilde{H}_\sigma, F_\sigma]), \text{ where } \tilde{H}_\sigma \equiv C_\sigma^\dagger H_\sigma C_\sigma.$$

In summary, we have the following expressions for the LSDA Lagrangian and derivatives

$$\begin{aligned} \mathcal{L}_{LSDA}(Y_\uparrow, Y_\downarrow, \phi) &= -\frac{1}{2} \sum_\sigma \text{Tr} (F_\sigma C_\sigma^\dagger L C_\sigma) + \frac{1}{8\pi} \phi^\dagger L \phi \\ &\quad + (\mathcal{J} n)^\dagger [V_{ion} + \mathcal{O} \mathcal{J} \epsilon_{xc}(n_\uparrow, n_\downarrow) - \bar{\mathcal{O}} \phi] \\ \frac{\partial \mathcal{L}_{LSDA}}{\partial Y_\sigma^\dagger} &= (I - \mathcal{O} C_\sigma C_\sigma^\dagger) H_\sigma C_\sigma F_\sigma U_\sigma^{-1/2} + \mathcal{O} C_\sigma Q([\tilde{H}_\sigma, F_\sigma]) \\ \frac{\partial \mathcal{L}_{LSDA}}{\partial \phi^\dagger} &= -\frac{1}{2} \bar{\mathcal{O}} \mathcal{J} n + \frac{1}{8\pi} L \phi. \end{aligned}$$

5.2 Self-interaction correction

The LDA and LSDA exchange-correlation functionals suffer from self-interaction errors: the functionals do not correctly subtract away the interaction of an electron with its own Hartree field when the electron density is not uniform. Perdew and Zunger [12] proposed a scheme to correct for these errors (the SIC-LDA which we simply refer to as SIC below).

The idea is to subtract the individual electrostatic and exchange-correlation contributions due to the density $n_i(r) = \|\psi_i(r)\|^2$ of each quantum state $\psi_i(r)$ from the LDA functional. This procedure has the virtue of yielding the correct result for a one-electron system as well as correcting for the Hartree self-interaction exactly. In terms of our formalism, we define the density matrix P_i and electron density n_i for the state i and relate them to the total density matrix P and total electron density n through

$$P_i = C e_i f_i e_i^\dagger C^\dagger, \quad P = \sum_i P_i; \quad n_i = \text{diag}(\mathcal{I} P_i \mathcal{I}^\dagger), \quad n = \sum_i n_i,$$

where e_i is the column vector with unity in the i th entry and zero elsewhere. In addition to the total Hartree field ϕ , we also introduce Hartree fields ϕ_i for each state i , and the SIC Lagrangian takes the form

$$\begin{aligned} \mathcal{L}_{SIC}(C, \{\phi_i\}) &= -\frac{1}{2} \text{Tr} (F C^\dagger L C) + (\mathcal{J} n)^\dagger [V_{ion} + \mathcal{O} \mathcal{J} \epsilon_{xc}(n) - \bar{\mathcal{O}} \phi] + \frac{1}{8\pi} \phi^\dagger L \phi \\ &\quad - \sum_i (\mathcal{J} n_i)^\dagger [\mathcal{O} \mathcal{J} \epsilon_{xc}(n_i) - \bar{\mathcal{O}} \phi_i] - \frac{1}{8\pi} \sum_i \phi_i^\dagger L \phi_i. \end{aligned}$$

Setting the variation with respect to ϕ_i and ϕ to zero (cf. Section 4.6) results in the Poisson equations

$$L\phi = 4\pi\bar{\mathcal{O}}\mathcal{J}n, \quad L\phi_i = 4\pi\bar{\mathcal{O}}\mathcal{J}n_i.$$

Substituting these solutions into the SIC Lagrangian yields the familiar SIC energy

$$\begin{aligned} E_{SIC}(C) = & -\frac{1}{2}\text{Tr}(FC^\dagger LC) + (\mathcal{J}n)^\dagger \left[V_{ion} + \mathcal{O}\mathcal{J}\epsilon_{xc}(n) - \frac{1}{2}\bar{\mathcal{O}}(4\pi L^{-1}\bar{\mathcal{O}}\mathcal{J}n) \right] \\ & - \sum_i (\mathcal{J}n_i)^\dagger \left[\mathcal{O}\mathcal{J}\epsilon_{xc}(n_i) - \frac{1}{2}\bar{\mathcal{O}}(4\pi L^{-1}\bar{\mathcal{O}}\mathcal{J}n_i) \right]. \end{aligned}$$

The derivatives of the SIC Lagrangian with respect to the density matrices P_i generate state-dependent Hamiltonians H_i and state-dependent potentials V_i given by

$$\begin{aligned} H_i &= -\frac{1}{2}L + \mathcal{I}^\dagger [\text{Diag}(V_{sp} - V_i)] \mathcal{I}, \\ V_i &= \mathcal{J}^\dagger \mathcal{O}\mathcal{J}\epsilon_{xc}(n_i) + [\text{Diag } \epsilon'_{xc}(n_i)] \mathcal{J}^\dagger \mathcal{O}\mathcal{J}n_i - \mathcal{J}^\dagger \bar{\mathcal{O}}\phi_i, \end{aligned}$$

where the state-independent potential V_{sp} is that of Eq. (36). The derivation of the expression for the derivative of the Lagrangian with respect to Y follows precisely the same steps as in Section 4.5.1, and the final form is

$$\begin{aligned} \left(\frac{\partial \mathcal{L}_{SIC}}{\partial Y^\dagger} \right) &= (I - \mathcal{O}CC^\dagger) \left(\sum_i H_i C e_i f_i e_i^\dagger \right) U^{-1/2} + \mathcal{O}CQ \left(\sum_i [\tilde{H}_i, e_i f_i e_i^\dagger] \right), \\ \tilde{H}_i &= C^\dagger H_i C. \end{aligned}$$

An examination of this form shows that to compute the derivative, each Hamiltonian H_i need only be applied to the i th column of C (as the product $C e_i$ occurs in all places), so that computation of the derivative is only slightly more demanding than the corresponding LDA derivative.

The above results for the derivative are a generalization of those in [13]. Those authors, however, work in the traditional real-space representation (where necessarily all the sums over indices appear) and, at each step of the minimization, orthonormalize their wave functions, so that their expressions are a special case of ours when $U = I$.

The summary of the SIC Lagrangian and derivatives follows.

$$\begin{aligned} \mathcal{L}_{SIC}(Y, \phi, \{\phi_i\}) &= -\frac{1}{2}\text{Tr}(FC^\dagger LC) + (\mathcal{J}n)^\dagger \left[V_{ion} + \mathcal{O}\mathcal{J}\epsilon_{xc}(n) - \bar{\mathcal{O}}\phi \right] \\ &\quad - \sum_i (\mathcal{J}n_i)^\dagger \left[\mathcal{O}\mathcal{J}\epsilon_{xc}(n_i) - \bar{\mathcal{O}}\phi_i \right] + \frac{1}{8\pi}\phi^\dagger L\phi - \frac{1}{8\pi} \sum_i \phi_i^\dagger L\phi_i, \\ \frac{\partial \mathcal{L}_{SIC}}{\partial Y^\dagger} &= (I - \mathcal{O}CC^\dagger) \left(\sum_i H_i C e_i f_i e_i^\dagger \right) U^{-1/2} + \mathcal{O}CQ \left(\sum_i [\tilde{H}_i, e_i f_i e_i^\dagger] \right), \\ \frac{\partial \mathcal{L}_{SIC}}{\partial \phi^\dagger} &= -\frac{1}{2}\bar{\mathcal{O}}\mathcal{J}n + \frac{1}{8\pi}L\phi, \quad \frac{\partial \mathcal{L}_{SIC}}{\partial \phi_i^\dagger} = \frac{1}{2}\bar{\mathcal{O}}\mathcal{J}n_i - \frac{1}{8\pi}L\phi_i. \end{aligned}$$

5.3 Band-structure and fixed Hamiltonian calculations

Very often, we aim to find a set of quantum states $\{\psi_i\}$ that are the lowest energy eigenstates of a fixed Hamiltonian. One case where this occurs is in the calculation of band structures for solids within DFT, where one has already found the stationary point of the Lagrangian and the optimal electron density $n(r)$. One then aims to explore the band structure for various values of k -vectors. (See Appendix C for a full discussion of k -points.) This requires finding the lowest energy eigenstates of the Hamiltonian. The problem is the same as a tight-binding calculation in the sense that the Hamiltonian is fixed and the electronic energy of the system is sought after, i.e. the minimum of the expectation value of the Hamiltonian among an orthonormal set of states. In both cases, the approach described below is most useful when the number of basis functions is much larger than the number of states $\{\psi_i\}$ so that direct diagonalization of the Hamiltonian is computationally prohibitive.

In such cases, we have a Hamiltonian H , and we expand our wave functions as shown in Eq. (7). We must minimize the energy E

$$E = \text{Tr}(C^\dagger H C).$$

We introduce unconstrained variables Y in the same way as before (Eq. (31) and onwards). The variation of the energy is given by

$$dE = \text{Tr}(H d[YU^{-1}Y^\dagger]) = 2 \text{Re} \text{Tr} \left[dY^\dagger \left(\frac{\partial E}{\partial Y^\dagger} \right) \right],$$

where the derivative of E is

$$\left(\frac{\partial E}{\partial Y^\dagger} \right) = (I - OCC^\dagger)HCU^{-1/2}.$$

When we are at the minimum of E , we have an orthonormal set C that spans the subspace of the lowest-energy eigenstates of H . The minimum value of E is the electronic energy for the case of a tight-binding Hamiltonian. If the energy eigenvalues and eigenvectors are desired, we diagonalize the subspace Hamiltonian $\tilde{H} = C^\dagger H C$ to obtain the eigenvalues ϵ . We then use the unitary matrix S which diagonalizes \tilde{H} , $\tilde{H} = S(\text{Diag } \epsilon)S^\dagger$, to find the expansion coefficients for the eigenstates, given by the product CS . The summary of key equations follows.

$$\begin{aligned} E(Y) &= \text{Tr}(C^\dagger H C), \\ \frac{\partial E}{\partial Y^\dagger} &= (I - OCC^\dagger)HCU^{-1/2}. \end{aligned}$$

5.4 Unoccupied states

A slightly more complex variant of the previous problem arises when we have converged a calculation, found the orthonormal states C spanning the occupied subspace, and are interested in finding the eigenvalues and eigenstates for the low-lying unoccupied states. For

example, let us say that we have converged a calculation in an insulator or semi-conductor, where the occupied space specifies the valence band. We wish to find the low-lying conduction states in order to study the band structure and band-gap of the material.

Thus, we start with a fixed Hamiltonian H and a fixed set of occupied states C . We aim to find a set of orthonormal unoccupied states D that are orthogonal to C and which also minimize the expectation of the Hamiltonian. Specifically, we wish to minimize $E = \text{Tr}(D^\dagger H D)$ under the orthogonality constraint $D^\dagger \mathcal{O} C = 0$.

We introduce a set of unconstrained states Z . We project out the part of Z lying in the occupied subspace by using the projection operator $\bar{\rho}^\dagger = I - C C^\dagger \mathcal{O}$ of Section 4.6,

$$D = \bar{\rho}^\dagger Z X^{-1/2} \quad \text{where} \quad X = (\bar{\rho}^\dagger Z)^\dagger \mathcal{O} (\bar{\rho}^\dagger Z).$$

Then, following the results of the previous section, the differential of E is given by

$$dE = \text{Tr}(H d[\bar{\rho}^\dagger Z X^{-1} \bar{\rho} Z^\dagger]) = 2 \text{Re} \text{Tr} \left[dZ^\dagger \left(\frac{\partial E}{\partial Z^\dagger} \right) \right],$$

where the derivative of E with respect to Z is given by

$$\left(\frac{\partial E}{\partial Z^\dagger} \right) = (I - \mathcal{O} C C^\dagger)(I - \mathcal{O} D D^\dagger) H D X^{-1/2}.$$

As expected, the derivative has two projection operators: $\bar{\rho} = I - \mathcal{O} C C^\dagger$, which projects out the component lying in the occupied subspace, and $(I - \mathcal{O} D D^\dagger)$, which projects out the component lying in the portion of the unoccupied subspace under consideration. Minimization of E leads to a set of states D that span the lowest-lying unoccupied states. At the minimum, the resulting unoccupied subspace Hamiltonian $\bar{H} = D^\dagger H D$ can be diagonalized to obtain the desired eigenvalues and eigenstates.

The energy and its gradient are summarized by

$$\begin{aligned} E(Z) &= \text{Tr}(D^\dagger H D), \\ \frac{\partial E}{\partial Z^\dagger} &= (I - \mathcal{O} C C^\dagger)(I - \mathcal{O} D D^\dagger) H D X^{-1/2}, \\ D &= \bar{\rho}^\dagger Z X^{-1/2} \quad , \quad X = (\bar{\rho}^\dagger Z)^\dagger \mathcal{O} (\bar{\rho}^\dagger Z) \quad , \quad \bar{\rho} = I - \mathcal{O} C C^\dagger. \end{aligned}$$

5.5 Variational density-functional perturbation theory

In this final application, we consider perturbation theory within a single-particle formalism, which is required to compute response functions. Specifically, we consider the important case of linear response, which was first dealt with in [14]. We imagine that we have converged the calculation of the zeroth-order (i.e. unperturbed) configuration and have found the zeroth-order wave functions C_0 for our problem. We now wish to find the first-order changes of the wave functions, C_1 , due to an external perturbation to the system. Depending on the type of perturbation applied, the variation C_1 allows for the calculation of the corresponding response functions. For example, the displacement of atoms along a phonon mode allows for

the computation of the dynamical matrix for that mode whereas perturbations due to an external electrostatic field allow for calculation of the dielectric tensor.

Regardless of the physical situation, all perturbations enter as a change in the ionic (or external) potential V_{ion} which drives the electronic system. Letting λ be the perturbation parameter, we expand any physical quantity A in powers of λ and let A_n be the coefficient of λ^n in the expansion. A few examples follow

$$\begin{aligned} V_{ion} &= V_{ion,0} + \lambda V_{ion,1} + \lambda^2 V_{ion,2} + \dots \\ C &= C_0 + \lambda C_1 + \lambda^2 C_2 + \dots \\ n &= n_0 + \lambda n_1 + \lambda^2 n_2 + \dots \end{aligned}$$

As is well known from perturbation theory, the first order change $V_{ion,1}$ determines the first order shift of the wave functions C_1 .

The work of [14] shows that C_1 can be obtained via the constrained minimization of an auxiliary quadratic functional of C_1 . In our matrix-based notation, for the case of constant fillings (taken to be unity) and the LDA approximation, this quadratic functional is given by

$$\begin{aligned} E(C_1) &= \text{Tr} \left\{ C_1^\dagger H_0 C_1 - C_1^\dagger \mathcal{O} C_1 [\text{Diag } \epsilon_0] \right\} \\ &+ (\mathcal{J} n_1)^\dagger \left\{ V_{ion,1} + \mathcal{O} \mathcal{J} [\text{Diag } a(n_0)] n_1 - \frac{1}{2} \bar{\mathcal{O}} \phi_1 \right\} + E_{nonvar} . \end{aligned}$$

The energy E_{nonvar} contains terms that depend only on C_0 or the Ewald sum over atomic positions and need not concern us any further. The zeroth-order Hamiltonian $H_0 = -\frac{1}{2}L + \mathcal{I}^\dagger [\text{Diag } V_0] \mathcal{I}$ is the same as that of Eq. (36) where we have simply renamed the zeroth-order single-particle potential to V_0 . The diagonal matrix $\text{Diag } \epsilon_0$ holds the eigenvalues of the zeroth-order Hamiltonian. The vector $a(n_0)$ is found by evaluating the function $a(n) = \frac{d^2}{dn^2} (n \epsilon_{xc}(n))$ on the zeroth-order electron density n_0 over the real-space grid. The vector n_1 , the first order shift of the electron density, is given by

$$n_1 = 2 \text{ Re } \text{diag} \left(\mathcal{I} C_0 C_1^\dagger \mathcal{I}^\dagger \right) .$$

The first order change of the Hartree potential ϕ_1 is the solution of the Poisson equation $\phi_1 = 4\pi L^{-1} \bar{\mathcal{O}} \mathcal{J} n_1$.

Given the quadratic nature of $E(C_1)$, its differential with respect to C_1 follows immediately and is given by

$$dE = 2 \text{ Re } \text{Tr} \left\{ dC_1^\dagger \left(H_0 C_1 - \mathcal{O} C_1 [\text{Diag } \epsilon_0] + \mathcal{I}^\dagger [\text{Diag } V_1] \mathcal{I} C_0 \right) \right\} ,$$

where the first-order single-particle potential V_1 is given by

$$V_1 = \mathcal{J}^\dagger V_{ion,1} + \mathcal{J}^\dagger \mathcal{O} \mathcal{J} [\text{Diag } a(n_0)] n_1 + [\text{Diag } a(n_0)] \mathcal{J}^\dagger \mathcal{O} \mathcal{J} n_1 - \mathcal{J}^\dagger \bar{\mathcal{O}} \phi_1 .$$

The constraint to be obeyed during the minimization is that the first-order shifts C_1 be orthonormal to the zeroth-order wave functions C_0 ,

$$C_1^\dagger \mathcal{O} C_0 = I .$$

This constraint is easily handled in the manner of the previous section by using a projection operator. We introduce an unconstrained set of wave functions Y_1 from which we project out the part laying in the space spanned by C_0 ,

$$C_1 = (I - C_0 C_0^\dagger \mathcal{O}) Y_1.$$

Based on this relation, we find the gradient of E with respect to Y_1

$$dE = 2 \operatorname{Re} \operatorname{Tr} \left\{ dY_1^\dagger \left(\frac{\partial E}{\partial Y_1^\dagger} \right) \right\} \text{ where}$$

$$\left(\frac{\partial E}{\partial Y_1^\dagger} \right) = (I - \mathcal{O} C_0 C_0^\dagger) \left\{ H_0 C_1 - \mathcal{O} C_1 [\operatorname{Diag} \epsilon_0] + \mathcal{I}^\dagger [\operatorname{Diag} V_1] \mathcal{I} C_0 \right\}.$$

Finally, we can convert the energy function into a Lagrangian by letting ϕ_1 be a free variable and by adding the appropriate Hartree self-energy and coupling to n_1 . We arrive at the summarized expressions

$$\begin{aligned} \mathcal{L}(Y_1, \phi_1) &= \operatorname{Tr} \left\{ C_1^\dagger H_0 C_1 - C_1^\dagger \mathcal{O} C_1 [\operatorname{Diag} \epsilon_0] \right\} + E_{nonvar} \\ &\quad + (\mathcal{J} n_1)^\dagger \left\{ V_{ion,1} + \mathcal{O} \mathcal{J} [\operatorname{Diag} a(n_0)] n_1 - \bar{\mathcal{O}} \phi_1 \right\} + \frac{1}{8\pi} \phi_1^\dagger L \phi_1, \\ \frac{\partial \mathcal{L}}{\partial Y_1^\dagger} &= (I - \mathcal{O} C_0 C_0^\dagger) \left\{ H_0 C_1 - \mathcal{O} C_1 [\operatorname{Diag} \epsilon_0] + \mathcal{I}^\dagger [\operatorname{Diag} V_1] \mathcal{I} C_0 \right\}, \\ \frac{\partial \mathcal{L}}{\partial \phi_1^\dagger} &= -\frac{1}{2} \bar{\mathcal{O}} \mathcal{J} n_1 + \frac{1}{8\pi} L \phi_1. \end{aligned}$$

6 Minimization algorithms

In this section, we show how the DFT++ formalism can succinctly specify the algorithm which finds the stationary point of the Lagrangian or energy function (derived in the previous sections). Such an algorithm only requires the value and derivative of the objective function, which is the reason that we have repeatedly emphasized the importance of these two quantities in our analysis above. Once we choose a minimization algorithm, we need only “plug in” the objective function and its derivative into the appropriate slots. Furthermore, since the DFT++ formalism is compact and at the same time explicit, once we specify the operations that must be performed for a given algorithm in our notation, the transition to coding on a computer is trivial: the formulae translate directly into computer code (as shown in Section 7).

Specifically, we aim to find the stationary point of the Lagrangian of Eq. (28) with respect to Y and ϕ and possibly B . A direct search for the stationary point is possible, and at the saddle point, both the Kohn-Sham and Poisson equations hold true simultaneously. This highly effective strategy has been followed in [6]. Alternatively, other approaches to reach a solution of these equations through self-consistent iteration and use of Broyden-like schemes [15] may be considered.

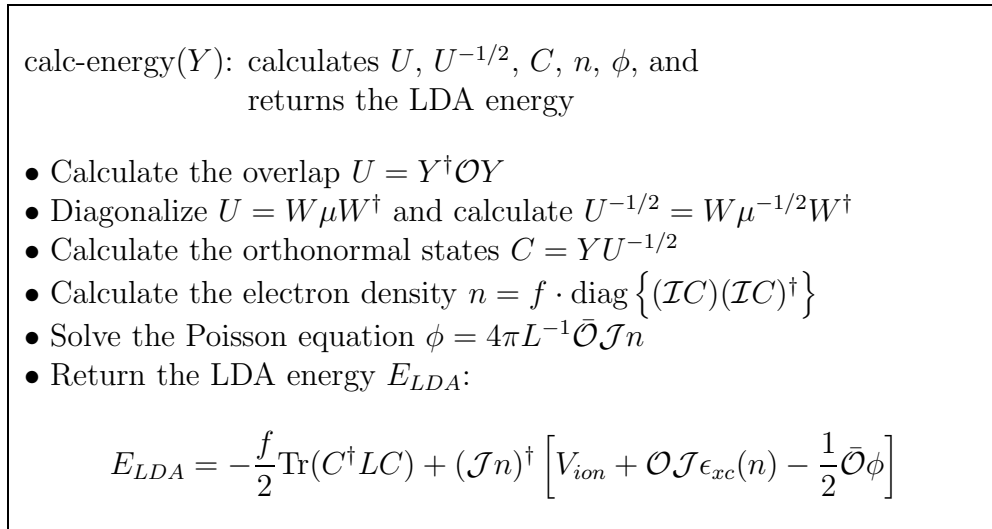


Figure 2: LDA energy routine (DFT++ formalism)

However, in order to make direct contact with DFT calculations within the traditional minimization context [7], and to keep our presentation as simple as possible, we choose instead to solve the Poisson equation (Eq. (42)) for the optimal ϕ at each iteration of the minimization algorithm. For cases where L^{-1} is easy to compute (e.g. the plane-wave basis where L is diagonal), we may compute the solution ϕ directly from Eq. (43). Otherwise, the straightforward approach of maximizing the quadratic functional $\mathcal{G}(\phi) = (1/8\pi) \phi^\dagger L \phi - (\mathcal{J} n)^\dagger \bar{\mathcal{O}} \phi$ via conjugate gradients (or some other method) achieves the same goal. For certain basis sets, multigrid methods or other specialized techniques are possibilities as well [6, 16, 17]. Once the Poisson equation has been solved, the remaining free variable is the matrix of coefficients Y , and the aim of the calculation is to minimize the energy E_{LDA} of Eq. (44) with respect to Y .

As shown in Section 3, the value and Y -derivatives of the Lagrangian \mathcal{L}_{LDA} and energy E_{LDA} are identical if we evaluate the Lagrangian-based expressions using the Hartree potential ϕ which is the solution of Poisson's equation. Therefore, in our algorithms below, we can use expressions derived for derivatives of the Lagrangian when dealing with the energy.

6.1 Semiconducting and insulating systems

Consider the case of a semiconducting system with a large unit cell. The fillings are constant, $F = fI$, and we will use a single k -point at $k = 0$ (as appropriate for a large cell). The simplest algorithm for minimizing the energy is the steepest descent method: we update Y by shifting along the negative gradient of the energy with respect to Y , scaled by a fixed multiplicative factor. As a first organizational step, we introduce the function calc-energy(Y), whose code we display in Figure 2. Given Y , this function computes the overlaps U and $U^{-1/2}$, the orthonormalized C , the electron density n , the solution to Poisson's equation ϕ , and returns the LDA energy. Figure 3 displays the steepest descent algorithm as it appears in the DFT++ language.

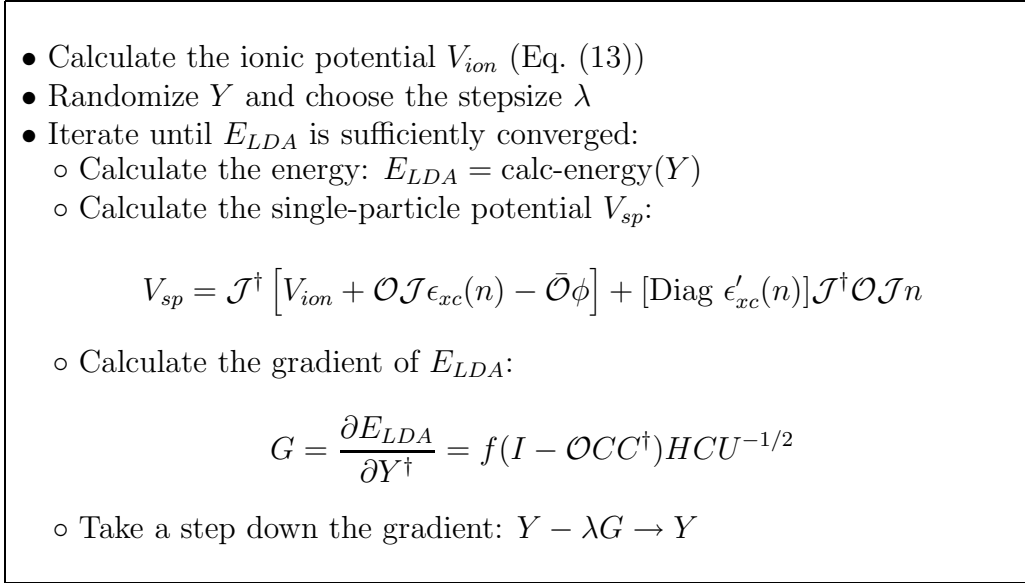


Figure 3: Steepest descent algorithm

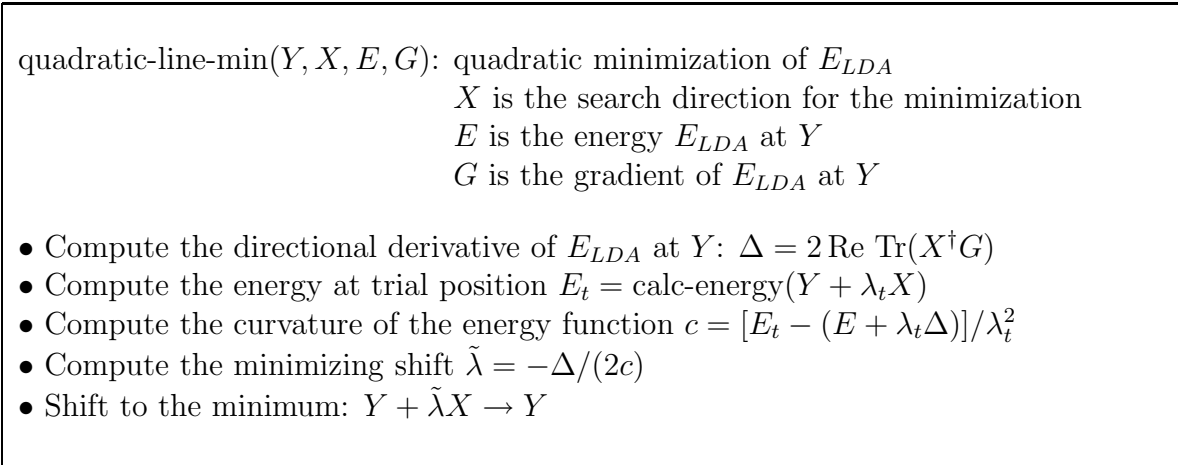


Figure 4: Quadratic line minimizer

We would like to emphasize a number of points regarding this code. First, the algorithm optimizes all the wave functions (i.e. the entire matrix Y) at once, leading to a very effective minimization and a complete avoidance of charge creep [1] or other instabilities. Second, the code is independent of the basis set used: the basis-dependent operators L , \mathcal{O} , etc., are coded as low-level functions that need to be written only once. The choice of physical system and minimization algorithm is a high-level matter that is completely decoupled from such details. Third, the figure shows *all* the operations required for the entire minimization loop. That this is possible is grace to the succinct matrix formalism.

The only part of the algorithm of Figure 3 that is specific to the steepest descent method is the last operation where Y is updated. To generalize to a preconditioned conjugate-gradient algorithm is quite straightforward, and we specify the necessary changes below.

- Calculate the ionic potential V_{ion}
- Randomize Y_0
- For $j=0, 1, 2, \dots$
 - Let $E_j = \text{calc-energy}(Y_j)$
 - Calculate the single-particle potential V_{sp}
 - Calculate the gradient: $G_j = (\partial E_{LDA}/\partial Y^\dagger)|_{Y_j}$
 - Apply the preconditioner: $\Gamma_j = K(G_j)$
 - If $j > 0$ then set $\alpha_j = \text{Re Tr}(G_j^\dagger \Gamma_j) / \text{Re Tr}(G_{j-1}^\dagger \Gamma_{j-1})$; otherwise $\alpha_j = 0$.
 - Compute the search direction $X_j = \Gamma_j + \alpha_j X_{j-1}$
 - Call quadratic-line-min(Y_j, X_j, E_j, G_j)

Figure 5: Preconditioned conjugate-gradient algorithm

Conjugate-gradient algorithms require line minimization of the objective function along a specified direction, i.e. an algorithm is needed that minimizes $E(\lambda) \equiv E_{LDA}(Y + \lambda X)$ with respect to the real number λ for a fixed search vector X . The subject of line minimization is rich, and an abundance of algorithms with varying degrees of complexity exist in the literature. (For a brief introduction see [18].) However, for typical DFT calculations, most of the effort for the calculation is spent in the quadratic basin close to the minimum. Thus, a simple and efficient line-minimizer that exploits this quadratic behavior should be sufficient, and we have found this to be the case in our work.

Our line-minimizer takes the current value of the energy and its derivative as well as the value of the energy at the shifted trial configuration $Y + \lambda_t X$ (where λ_t is a trial step-size) to achieve the quadratic fit $E(\lambda) \approx E + \Delta\lambda + c\lambda^2$. Here, Δ is the directional derivative of E with respect to λ , and c is the curvature of E with respect to λ . The line-minimizer then moves to the minimum of this quadratic fit located at $\tilde{\lambda} = -\Delta/(2c)$. Figure 4 shows the code for this line-minimizer.

Using this line minimizer, we present the entire preconditioned conjugate-gradient algorithm in Figure 5. Note that we have omitted some of the formulae which are identical to those of Figure 3. A simple diagonal preconditioning, as described in [7], is quite effective for plane-wave basis sets, and the operator K is the preconditioner in the algorithm of the figure.

6.2 Metallic and high-temperature systems

While the degrees of freedom in the variable Y are sufficient to describe any electronic system, the convergence of minimization algorithms can be hampered by ill-conditioning of the physical system. A standard case of such a problem is when the Fermi-Dirac fillings f_i are not constant and some fillings are very small, a situation encountered when studying metals or high-temperature insulators.

One type of ill-conditioning that arises due to states with small fillings, $f_i \ll 1$, stems from the fact that changes in such states do not affect the value of the energy E_{LDA} very

much when compared to the states with large fillings, $f_i \sim 1$. Thus modes associated with the small-filling states are “soft” and we have an ill-conditioned problem. The solution to this problem, however, is rather straightforward and involves scaling the derivative of \mathcal{L}_{LDA} with respect to the state ψ_i by $1/f_i$.

Much harder to deal with are soft modes due to subspace rotations which were introduced in Section 4.4. As we saw there, the unitary transformations V , which generate the rotations, cancel out completely from the expression for the density matrix P in the case of constant Fermi fillings, $F = fI$. Since the entire energy can be computed from P alone, the energy will not depend on V . Hence we have found that the unitary transformations V are an exact symmetry of a system with constant fillings.

However, once we introduce variations in the fillings, the symmetry is broken. Now both the density matrix and the energy change when V mixes states with different fillings. If the difference in fillings between the mixed states is small, a case typically encountered in a real system, the mixing produces small changes in the energy. Again, we have soft modes, this time due to the breaking of the unitary subspace-rotation symmetry.

The idea of using subspace rotations was first suggested in [1]. Its use as a cure for the ill-conditioning described above was discussed and demonstrated convincingly in [19]. The strategy is first to minimize the objective function over B (since B parameterizes the rotation V) and only then perform minimization on the wave functions Y . By ensuring that we are always at the minimum with respect to B , we automatically set the derivative of E_{LDA} with respect to subspace-rotations to zero. When this is true, changing Y can not (to first order) give rise to contributions due to the soft modes, and we have eliminated the ill-conditioning.

In practice, we have found it unnecessary for our calculations to be at the absolute minimum with respect to B : being close to the minimum is sufficiently beneficial computationally. In our algorithm, we take steps along both Y and B simultaneously but ensure that our step-size in B is much larger than that in Y . As the minimization proceeds, this choice automatically drives the system to stay close to the minimum along B at all times.

Our simpler procedure has been found as effective as the original strategy of [19] and translates into using the following search direction X in the space (Y, B)

$$X = \left(\frac{\partial \mathcal{L}_{LDA}}{\partial Y^\dagger}, \eta \cdot \frac{\partial \mathcal{L}_{LDA}}{\partial B} \right)$$

where η is a numerical scaling factor. We have found $\eta \sim 30$ to be a good choice for efficient minimization while avoiding the ill-conditioning mentioned above.

As a practical showcase of the improvement in convergence in a metallic system, we study the convergence rate for the conjugate-gradient minimization of the energy of bulk molybdenum. We study the bcc cubic unit cell containing two Mo atoms. We use a plane-wave basis set (details of implementation in Appendix A) with an electronic cutoff of 22.5 Hartree (45 Ryd), and a $4 \times 4 \times 4$ cubic k -point mesh to sample the Brillouin zone. The electronic temperature used is $k_B T = 0.0037$ Hartree (0.1 eV), the Fermi fillings are recomputed every twenty conjugate-gradient steps based on the eigenvalues of the subspace Hamiltonian from the previous iteration, and a value of $\eta = 30$ is used to calculate the search direction. Non-local pseudopotentials of the Kleinmann-Bylander form [20] are used with p and d projectors. Figure 6 presents a plot of the convergence of the energy per atom to

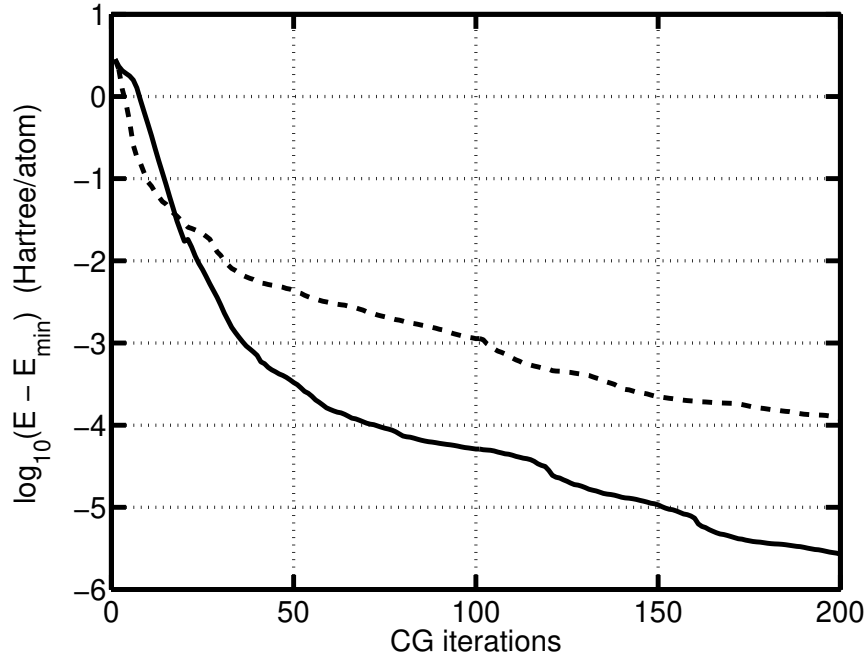


Figure 6: Effect of subspace rotation on convergence – Convergence of conjugate-gradient minimization with (solid) and without (dashed) the use of subspace rotations for the case of a metallic system. Both minimizations use the same random wave functions as their starting points. The horizontal axis is the number of conjugate-gradient iterations and the vertical axis is the energy per atom above the minimum energy in Hartree per atom in logarithmic units. See the text for further details.

its minimum value (as determined by a run with many more iterations than shown in the figure). We compare minimization with and without the use of subspace rotation variables, and both minimizations are started with the same initial random wave functions. The extra cost required for the use of subspace rotations was very small in this case, the increase in the time spent per iteration being less than two percent. As we can see, the use of subspace rotations dramatically improves the convergence rate.

7 Implementation, optimization, and parallelization

In this final section we address how the DFT++ formalism can be easily and effectively implemented on a computer, and what steps must be taken to ensure efficient optimization and parallelization of the computations. As is clear from the previous sections, the DFT++ formalism is firmly based on linear algebra. The objects appearing in the formalism are vectors and matrices. The computations performed on these objects are matrix addition and multiplication and the application of linear operators. An important benefit is that linear-algebraic products involve matrix-matrix multiplications (i.e. BLAS3 operations), which are precisely those operations that achieve the highest performance.

We use an object-oriented approach and the C++ programming language to render the implementation and coding as easy as possible. In addition, object-oriented program-

ming introduces modularity and localization of computational kernels allowing for effective optimization and parallelization. In the sections below, we present outlines of our implementation, optimization, and parallelization strategies.

7.1 Object-oriented implementation in C++

In our work, we have found that an object-oriented language such as C++ is ideal for implementing the required vectors and matrices and for defining the operations on them in a manner that follows the DFT++ formalism as closely as possible. The object-oriented approach presents a number of advantages.

First, the programming task becomes highly modular: we identify the object types needed and the operations that must be performed on them, and we create a separate module for each object that can be tested independently. For example, we define the class of matrices and the operations on them (e.g. multiplication, addition, diagonalization, etc.), and we can test and debug this matrix module separate from any other considerations. Second, we gain transparency: the internal structure or functioning of an object can be modified for improved performance without requiring any changes to higher-level functions that use the object. This gives us a key feature in that the high-level programmer creating new algorithms or testing new energy functionals does not need to know about or interact with the lower-level details of how the objects actually are represented or how they function. Third, this separation of high-level function from low-level implementation allows for a centralization and reduction in the number of computational kernels in the code: there can be a large variety of high-level objects for the convenience of the programmer, but as all the operations defined on them are similar linear-algebraic ones, only a few actual routines must be written. Fourth, modularity produces shorter and more legible code. This, combined with the object-oriented approach, implies that the high-level computer code will read the same as the equations of the DFT++ formalism so that debugging will amount to checking formulae, without any interference of cumbersome loops and indices.

To give a concrete example of what this means, consider the simplest object in the formalism, a column vector such as the electron density n . In C++, we define an object class `vector` which will contain an array of `complex` numbers (itself a lower-level object). A `vector v` has a member `v.size` specifying the number of rows it contains as well as a pointer to the array containing the data. We define the action of the parenthesis so as to allow convenient access of the i th element of v via the construction `v(i)`.

A very common operation between two vectors v and w is the scalar product $v^\dagger w$. We implement this by defining (in C++ parlance overloading) an operator `^` that takes two `vectors` and returns a `complex` result. The code accomplishing this is

```
friend complex operator^(vector &v, vector &w)
{
    complex result = 0;

    for(int i=0; i < v.size; i++)
        result += conjugate(v(i))*w(i);

    return result;
}
```

}

An example of an operator acting on vectors is the inverse transform \mathcal{J} . This operator can be coded as a function `J` that takes a `vector v` as its argument and returns the `vector` result `J(v)`. Of course, the details of what \mathcal{J} does internally are basis-dependent.

Based on this definition, the evaluation of the electron-ion interaction energy of Section 4.3.2, given by the expression $E_{e-i} = (\mathcal{J}n)^\dagger V_{ion}$, is coded by

```
E_ei = J(n)~V_ion;
```

where `V_ion` is the vector V_{ion} of Eq. (13).

Following the same idea, we define a `matrix` class to handle the matrices such as U , W , \tilde{H} , etc. that occur in the formalism. Physically, expansion coefficients such as Y and C are collections of column vectors (a column of coefficients $C_{\alpha i}$ for each wave function ψ_i), and we define the class `column_bundle` to handle these objects. Although mathematically `column_bundles` such as Y and C are matrices, the choice not to use the `matrix` class for representing them is deliberate, as Y and C have a distinct use and a special physical meaning that an arbitrary matrix will not have. In this way, we can tailor our objects to reflect the physical content of the information they contain. Of course, when a matrix multiplication is performed, such as when we evaluate the expression $C = YU^{-1/2}$, the `column_bundle` class and `matrix` class call a single, low-level, optimized multiplication routine. We thus gain flexibility and legibility of codes on the higher levels while avoiding an accumulation of specialized functions on the lower levels.

As a concrete example of the power and ease of this style of programming, consider writing the code for the function `calc-energy(Y)` of Figure 2. In order to do so, we will need a few more operators. Following the example of the `vectors`, we define the `~` operator between two `column_bundles` to handle Hermitian-conjugated multiplications such as $Y_1^\dagger Y_2$, where the result of the product is of type `matrix`. Next, we define the `*` operator between a `column_bundle` and `matrix` to handle multiplications of the type $YU^{-1/2}$, where the result is a `column_bundle`. We code the action of the basis-dependent operators such as \mathcal{O} or \mathcal{I} on a `vector` ϕ or a `column_bundle` C as function calls `O(phi)` or `I(C)`, which return the same data type as their argument. Finally, we implement multiplication by scalars in the obvious way. Figure 7 presents the C++ code for the energy calculation routine. The code is almost exactly the same as the corresponding expressions in the DFT++ formalism, making the translation from mathematical derivation to actual coding trivial.

7.2 Scalings for dominant DFT++ operations

Before we describe our approach to optimization and parallelization, we will work out the scalings of the floating-point operation counts as a function of system size for the various computational operations in the DFT++ formalism. Thus it will be clear which optimizations and parallelizations will increase the overall performance most efficaciously. Let n be the number of wave functions $\{\psi_i\}$ and let N be the number of basis functions $\{b_\alpha(r)\}$ in the calculation. A `vector` contains N complex numbers, a `matrix` is $n \times n$, and a `column_bundle` is $N \times n$ and is the largest data structure in the computation. Both n and N are proportional to the number of atoms n_a in the simulation cell, or equivalently, to the volume of the cell.

```

complex calc_energy(column_bundle &Y, column_bundle &C,
                    matrix &U, matrix &Umhalf,
                    vector &n, vector &phi,
                    double f, vector &V_ion)
{
    complex E_LDA;

    U = Y^0(Y);

    // calc_Umhalf(U) returns U^{-1/2} given U
    Umhalf = calc_Umhalf(U);

    C = Y*Umhalf;

    // diag_of_self_product(X) returns diag(X*adjoint(X))
    n = f*diag_of_self_product(I(C));

    phi = (4.0*PI)*invL(Obar(n));

    E_LDA = -0.5*f*Tr(C^L(C)) +
            J(n)^( V_ion + 0(J(exc(n))) - 0.5*Obar(phi) );

    return E_LDA;
}

```

Figure 7: LDA energy routine (C++ implementation) – C++ code for the `calc-energy(Y)` function which was outlined in Figure 2. When computing the electron density \mathbf{n} , we have not used the straightforward code `diag(X*adjoint(X))` which first computes the entire matrix $X*adjoint(X)$ before extracting its diagonal and is thus computationally wasteful. Rather, for performance reasons, we have written a separate function `diag_of_self_product(X)` that given a `column_bundle X` computes only the required diagonal portion of the product $X*adjoint(X)$.

Typically, for accurate DFT calculations, the number of basis functions required is much larger than the number of quantum states, $N \gg n$.

In Table 1 we present the floating-point operation counts for the different operations required in the DFT++ formalism. We note that for very large systems, the basis-set independent matrix products dominate the overall computational workload. However, for medium-sized or slightly larger problems, the application of the basis-dependent operators can play an important role as well.

For most basis sets, there are techniques available in the literature that allow for efficient application of the basis-dependent operators to a column vector in $O(N)$ or $O(N \ln N)$ operations. For example, when working with plane waves, the Fast Fourier transform [21]

Operation	Examples	FLOP count
column_bundle multiplications	$M = Y_1^\dagger Y_2$ or $C = YU^{-1/2}$	$O(n^2N)$
matrix multiplications and diagonalizations	$U = W\mu W^\dagger$ or $U^{-1/2} = W\mu^{-1/2}W^\dagger$	$O(n^3)$
Applying basis-dependent operators	$\mathcal{O}Y$, LC , or $\mathcal{I}C$	$O(nN)$ or $O(nN \ln N)$
Calculating n given $\mathcal{I}C$ or calculating the kinetic energy given LC	$n = \text{diag}\{\mathcal{I}C\}F(\mathcal{I}C)^\dagger\}$ or $\text{Tr}\{FC^\dagger(LC)\}$	$O(nN)$
vector operations	$\epsilon_{xc}(n)$, $(\mathcal{J}n)^\dagger V_{ion}$, or $\mathcal{O}\phi$	$O(N)$

Table 1: Floating-point operation count for various common operations in the DFT++ formalism. The size of the basis set is N and the number of wave functions is n . Thus a **column_bundle** is $N \times n$, a **matrix** is $n \times n$, and a **vector** is N long.

is the algorithm of choice for implementing the operators \mathcal{I} , \mathcal{J} , \mathcal{I}^\dagger , and \mathcal{J}^\dagger and allows us to affect these operators in $O(N \ln N)$ operations. (See Appendix A for the details of a plane-wave implementation.) The operators L and \mathcal{O} are already diagonal in a plane-wave basis and are thus trivial to implement. For real-space, grid-based computations, multigrid methods [16] are highly effective for inverting L and solving the Poisson equation. Special techniques exist for multiresolution [4, 6, 22] and Gaussian [17] basis sets that allow for the application of the basis-dependent operators in $O(N)$ operations as well.

7.3 Optimization of computational kernels

Due to the modularity of our object-oriented approach, the physical nature of the problem under study is a high-level issue that is completely independent of the functioning of the few, low-level computational kernels which handle most of the calculations in the code. The aim now is to optimize these kernels to obtain maximum computational performance. By optimization we mean increasing performance on a single processor. Parallelization, by which we mean distribution of the computational task among several processors, will be addressed in the next section, but good parallel performance is only possible when each processor is working most effectively.

The computationally intensive operations involved in the DFT++ formalism fall into two overall classes. First are the application of the basis-dependent operators such as L , \mathcal{O} , \mathcal{I} , etc., whose operation counts scale quadratically in the system size (see Table 1). Given their basis-dependent nature, no general recipe can be given for their optimization. However, for many widely used basis sets, highly efficient methods exist in the literature which allow for the application of these operators, and we refer the reader to the references cited in the preceding section. For the case of plane waves, we have used the FFTW package [3] to affect the Fourier transformations. This highly portable, freely obtainable software library

provides excellent per processor performance across many platforms.

The second class of operations are the basis-independent matrix products, and we will now consider the optimization of these operations. As a case study, we examine the Hermitian-conjugated matrix product between two `column_bundles`, which occurs in an expression such as $Y_1^\dagger Y_2$ and which is coded using the `column_bundle^column_bundle` operator as `Y_1^Y_2`. The most “naive” and straightforward implementation of this operator in C++ is given by

```
friend matrix operator^(column_bundle &Y_1, column_bundle &Y_2)
{
    // create a matrix of size Y_1.n_columns x Y_2.n_columns
    // to hold the result
    matrix M(Y_1.n_columns, Y_2.n_columns);
    int i, j, k;

    for(i=0; i < Y_1.n_columns; i++)
        for(j=0; j < Y_2.n_columns; j++) {
            M(i, j) = 0;
            for(k=0; k < Y_1.n_rows; k++)
                M(i, j) += conjugate(Y_1(k, i))*Y_2(k, j);
        }

    return M;
}
```

While easy to follow, this implementation is quite inefficient on modern computer architectures for large matrix sizes because the algorithm does not take any advantage of caching. The access pattern to memory is not localized, and the processor must continually read and write data to the slower-speed main memory instead of to the much faster (but smaller) cache memory.

One solution to this problem is to resort to vendor-specific linear algebra packages. For example, one can use a version of LAPACK optimized for the computational platform at hand, and this generally results in very good performance. An alternative choice is to perform the optimizations by hand. While this second choice may sacrifice some performance, it does ensure highly portable code, and this is the strategy that we have followed in our work.

Our basic approach to increasing performance is to use blocking: we partition each of the input and output matrices into blocks of relatively small dimensions, and the matrix multiplication is rewritten as a set of products and sums over these smaller blocks. Provided that the block sizes are small enough, say 32×32 or 64×64 for today’s typical processor and memory architectures, both the input and output blocks will reside in the high-speed cache memory and fast read/write access to the cache will dramatically improve performance. Figure 8 shows a schematic diagram of how the product $M = Y_1^\dagger Y_2$ would be carried out in a blocked manner.

Please note that due to blocking, the task of optimization is now also modularized. We need only write a single, low-level, block-block matrix multiplication routine that should be highly optimized. All higher-level matrix multiplication functions will then loop over

$$\begin{array}{ccc}
M & = & Y_1^\dagger Y_2 \\
\left(\begin{array}{c|c} m_{00} & m_{01} \\ \hline m_{10} & m_{11} \end{array} \right) & = & \left(\begin{array}{c|c|c|c} a_{00} & a_{01} & a_{02} & a_{03} \\ \hline a_{10} & a_{11} & a_{12} & a_{13} \end{array} \right) \times \left(\begin{array}{c|c} b_{00} & b_{01} \\ \hline b_{10} & b_{11} \\ \hline b_{20} & b_{21} \\ \hline b_{30} & b_{31} \end{array} \right) \\
& & m_{ij} = \sum_k a_{ik} b_{kj}
\end{array}$$

Figure 8: Blocked matrix multiplication – A schematic of the blocked matrix multiplication method applied to computing the product $M = Y_1^\dagger Y_2$. The blocks m_{ij} , a_{ij} , and b_{ij} are matrices of small size (e.g. 32×32). Our schematic shows how each of the matrices is partitioned into blocks and how the result blocks m_{ij} are to be computed.

blocks of the input and output data and copy the contents to small, in-cache matrices which are then multiplied by calling the low-level multiplier.

Applying these ideas to our $M = Y_1^\dagger Y_2$ example, the rewritten code for the `column_bundle^column_bundle` operator takes the following form:

```

friend matrix operator^(column_bundle &Y_1, column_bundle &Y_2)
{
    matrix M(Y_1.n_columns, Y_2.n_columns); // M=Y_1^Y_2 holds the result

    int B = 32; // Pick a reasonable block size

    matrix in1(B,B), in2(B,B), out(B,B); // input and output blocks

    int ib, jb, kb, i, j, k;

    // loop over blocks of the output
    for(ib=0; ib < Y_1.n_columns; ib+=B)
        for(jb=0; jb < Y_2.n_columns; jb+=B) {

            // zero the output block
            for(i=0; i < B; i++)
                for(j=0; j < B; j++)
                    out(i,j) = 0;

            // loop over blocks to be multiplied

```

```

for(kb=0; kb < Y_1.nrows; kb+=B) {

    // load data into input blocks
    for(i=0; i < B; i++)
        for(k=0; k < B; k++) {
            in1(i,k) = conjugate(Y_1(kb+k,ib+i));
            in2(i,k) = Y_2(kb+k,jb+i);
        }

    // perform the block multiplication
    low_level_multiply(in1, in2, out, B);
}

// write the result to memory
for(i=0; i < B; i++)
    for(j=0; j < B; j++)
        M(ib+i,jb+j) = out(i,j);
}

return M;
}

```

The function `low_level_multiply` performs the block-block multiplication of the input blocks and accumulates into the output block. Not only the `column_bundle^column_bundle` operator but *all* matrix multiplications can be blocked in a similar way and will thus call the low-level multiplier.

The simplest implementation for `low_level_multiply` is the straightforward one:

```

void low_level_multiply(matrix &in1, matrix &in2,
                       matrix &out, int B)
{
    int i,j,k;
    for(i=0; i < B; i++)
        for(j=0; j < B; j++) {
            complex z = 0;
            for(k=0; k < B; k++)
                z += in1(i,k)*in2(j,k);
            out(i,j) += z;
        }
}

```

The use of this simple low-level multiplier combined with blocking can provide a tremendous improvement. Figure 9 shows a plot of the performance of the $M = Y_1^\dagger Y_2$ blocked-multiplication as a function of the block size when run on a 333 MHz SUN Ultrasparc 5 microprocessor. For comparison, the performance of the “naive” code with no blocking, which was presented above, is also indicated in the figure. Initially, the performance increases

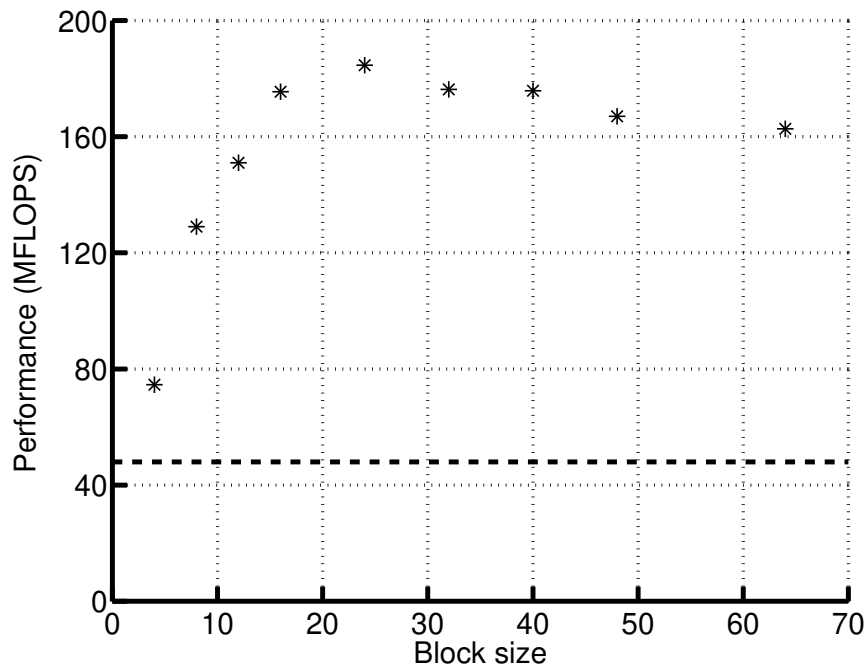


Figure 9: Matrix-multiplication FLOP rates (single processor) – Effect of blocking on computational performance for the matrix product $M = Y_1^T Y_2$, where Y_1 and Y_2 are $10,000 \times 200$ complex-valued matrices. The horizontal axis shows the size of the square blocks used for the block-multiplication scheme described in the text. The vertical axis is the performance in mega floating-point operations per second (MFLOPS). The horizontal dashed line shows the rate for a non-blocked “naive” multiplication routine (see text).

dramatically with increasing block size due to more effective caching. However, there is an optimal size above which performance decreases because the blocks become too large to fit effectively into the cache. On most computational platforms that we have had experience with, this simple blocked multiplier runs at at least half the peak theoretical rate of the processor, as exemplified by the results in the figure. Further speedups can be found by rewriting the `low_level_multiply` routine so as to use register variables (as we have done and found up to 40% performance enhancements) or by using a hierarchical access pattern to memory which can provide better performance if the memory system has multiple levels of caching.

7.4 Parallelization

Once the computer code has been optimized to perform well on a single processor, the computation can be divided among multiple processors. We now discuss how this division can be achieved effectively.

The architectures of modern parallel supercomputers can generally be divided into two categories: shared-memory (SMP) versus distributed-memory (DMP) processors. In the SMP case, a set of identical processors share access to a very large repository of memory. The main advantages of shared memory are that the processors can access whatever data they

need, and that, with judicious choice of algorithms, very little inter-processor communication is required. In addition, only small changes are required to parallelize a serial code: the computational task is divided among the processors, and each processor executes the original serial code on the portion of the data allotted to it. However, as the number of processors increases, the traffic for accessing the main memory banks increases dramatically and the performance will stop to scale well with the number of processors utilized. Nevertheless, many mid-sized problems are well suited to SMPs and can take full advantage of the key features of SMP systems. Examples of such calculations can be found in [23, 24].

The largest of today's supercomputers have distributed memory: each processor has a private memory bank of moderate size to which it has exclusive access, and the processors communicate with each other by some message passing mechanism. The main advantages of DMP are scalability and heterogeneity, as the processors need not all be identical nor located in close physical proximity. However, the price paid is the necessity of an inter-processor communication mechanism and protocol. In addition, computer algorithms may have to be redesigned in order to minimize the required communication. Furthermore, a slow communication network between processors can adversely affect the overall performance.

We will describe, in outline, the strategies we employ for both SMP and DMP architectures, and we will continue to examine the case of the `column_bundle^column_bundle` matrix multiplication as a specific example. As our results for actual calculations will demonstrate, we only need to parallelize two main operations in the entire code, (a) the application of basis-dependent operators such as \mathcal{I} or L to `column_bundles` (which is trivial) and (b) the matrix products involving `column_bundles` such as $Y_1^\dagger Y_2$ or $YU^{-1/2}$, to obtain excellent or highly satisfactory performance on SMP and DMP systems.

7.4.1 Shared-memory (SMP) architectures

Since all processors in an SMP computer have access to all the data in the computation, the parallelization of the basis-dependent operators is trivial. For example, the operation $\mathcal{I}C$ involves the application of \mathcal{I} to each column of C separately, and the columns can be divided equally among the processors. This leads to near perfect parallelization as none of the processors read from or write to the same memory locations.

Based on the discussion of Section 7.2, for large problems, the most significant gains for parallelization involve the basis-independent matrix-products. Below, we focus on the `column_bundle^column_bundle` operation as a case study. For this operation, it is impossible to distribute the task so that all processors always work on different memory segments. However, we divide up the work so that no two processors ever write to the same memory location: not only does this choice avoid possible errors due to the synchronizations of simultaneous memory writes, it also avoids performance degradation due to cache-flushing when memory is written to.

Consider the matrix product $M = Y_1^\dagger Y_2$, which we have implemented as a blocked matrix multiplication. Parallelization is achieved simply by assigning each processor to compute a subset of the output blocks. The main program spawns a set of subordinate tasks (termed threads) whose sole purpose is to compute their assigned output blocks and to write the results to memory. The main program waits for all threads to terminate before continuing onwards. Referring to Figure 8, this strategy corresponds to distributing the computation of

the blocks m_{ij} among the processors, and since memory is shared, all processors have access to all of the data describing Y_1 and Y_2 at all times. For large problem sizes, the overhead in spawning and terminating the threads is far smaller than the work needed to compute the results, so the simplicity of this strategy does not sacrifice performance.

We now present the code which accomplishes this parallelized matrix product in order to highlight the ease with which such parallelizations can be performed. In the interest of brevity, we assume that the number of columns of Y_1 is a multiple of the number of threads launched. Parallelization is affected by assigning different threads to compute different rows of the result $M = Y_1^\dagger Y_2$.

```

friend matrix operator^(column_bundle &Y_1, column_bundle &Y_2)
{
    matrix M(Y_1.n_columns,Y_2.n_columns); // M=Y_1^Y_2 holds the result

    int n_threads = 8; // a reasonable number of threads

    int thread_id[n_threads];
    int i, start, n;

    for (i=0; i < n_threads; i++) {

        // The set of rows of M that this thread should compute
        n = Y_1.n_columns/n_threads;
        start = i*n;

        // Launch a thread that runs the routine calc_rows_of_M
        // and pass it the remaining arguments. Store the thread ID.
        thread_id[i] = launch_thread(calc_rows_of_M, Y_1, Y_2, M,
                                    start, n);
    }

    // Wait for the threads to terminate
    for (i=0; i < n_threads; i++)
        wait_for_thread(thread_id[i]);

    return M;
}

```

The routine `calc_rows_of_M(Y_1,Y_2,M,start,n)` computes rows `start` through `start+n-1` of M , where $M=Y_1^\dagger Y_2$. The routine's algorithm is identical to that of the blocked multiplier presented in the previous section. The only change required is to have the `ib` loop index start at `start` and end at `start+n-1`.

We parallelize other matrix multiplications involving `column_bundles` analogously. In addition, we parallelize the application of the basis-dependent operators as discussed above. For a realistic study of performance and scaling, we consider a system of bulk silicon with 128 atoms in the unit cell. We use a plane-wave cutoff of 6 Hartrees (12 Ryd) which leads

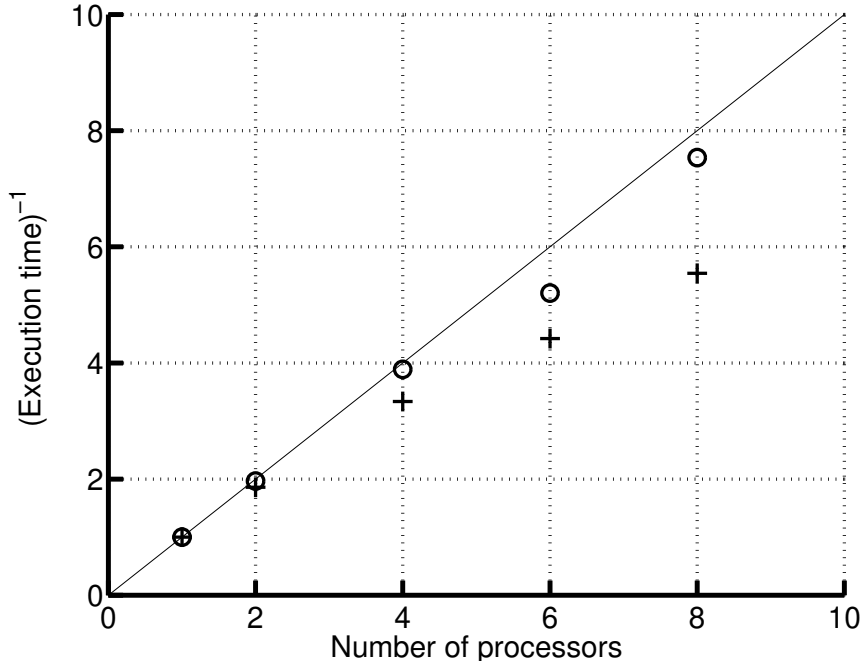


Figure 10: Scaling for SMP parallelization – Performance of our SMP parallelized plane-wave code for a 128 atom silicon system. We show the performance of the parallelized $M = Y_1^\dagger Y_2$ multiplications (circles) and the overall code (pluses) as a function of the number of processors. In both cases, performance has been normalized to the respective performance with a single processor. The straight line with slope of unity represents ideal scaling for perfect parallelization.

to a basis of size $N = 11797$. We use Kleinmann-Bylander [20] non-local pseudopotentials with p and d non-local projectors to eliminate the core states, and we have $n = 256$ bands of valence electrons. We sample the Brillouin zone at $k = 0$. In Figure 10, we show a plot of the performance of the parallelized $M = Y_1^\dagger Y_2$ multiplication as well as the overall performance of the code for a single conjugate-gradient step as a function of the number of processors employed. The calculation was run on a Sun Ultra HPC 5000 with eight 167 MHz Ultrasparc 4 microprocessors and 512MB of memory.

As the figure shows, the parallelized $M = Y_1^\dagger Y_2$ matrix multiplication shows near ideal scaling. There are a number of reasons for this behavior: (1) since different processors always write to different segments of memory, the algorithm does not suffer from memory write-contentions, (2) the inputs Y_1 and Y_2 are never modified so that memory reads are cached effectively, and (3) the problem size is large enough so that each processor’s workload is much larger than the overhead required to distribute the work among the processors. This scaling is all the more impressive because when using eight processors, each processor performs the multiplications at 140 MFLOPS or at 83% of the processor clock rate.

The figure also displays the total performance of the code, which shows evidence of saturation. To understand this behavior in more detail, we model the overall execution time in accordance with Amdahl’s law. We assume that there exists an intrinsic serial computation time T_0 which must be spent regardless of the number of processors available. In addition,

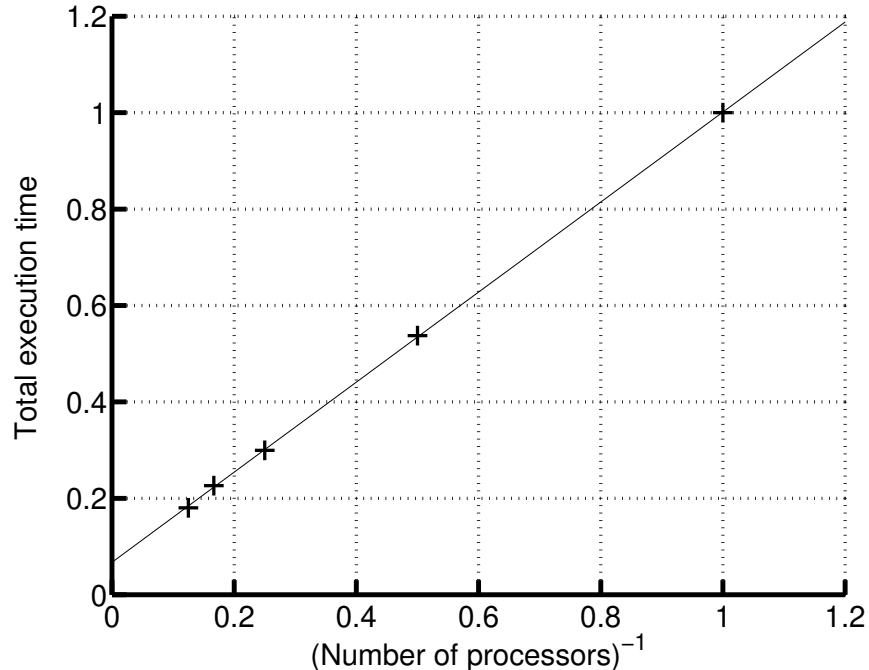


Figure 11: Amdahl’s analysis of SMP scaling – Total execution time of the SMP parallelized plane-wave code for a 128 silicon atom system as a function of the reciprocal of the number of processors used. The line of least-squares fit to the data points is also shown. Execution times are normalized in units of the execution time for a single processor.

there is an analogous parallel computation time \tilde{T} which, however, is divided equally among all the processors. Thus the total execution time will be given by $T = T_0 + \tilde{T}/p$, where p is the number of processors. We show a plot of the total execution time versus $1/p$ in Figure 11, and the model shows an excellent fit to the available data. The vertical asymptote of the least-squares fit straight line is the extrapolated value of T_0 , in this case approximately 10% of the single processor or serial execution time. Thus the few operations that we have chosen to parallelize do in fact constitute the largest share of the computational burden and our parallelization strategy is quite effective.

When we reach the data point with eight processors, the total execution time is already within a factor of two of T_0 , so that the total serial and parallel components have become comparable. Indeed, timing various portions of the code confirms this hypothesis: for example, with eight processors, the time needed to perform a parallel multiplication $M = Y_1^\dagger Y_2$ is equal to the time needed by the Sun high-performance LAPACK library to diagonalize the overlap matrix U (cf. Eq. (31)). With eight processors, the code has each processor *sustaining* an average of 134 MFLOPS or 80% of the processor clock rate. We are quite satisfied with this level of performance, but if more improvements are desired, the remaining serial portions of the code can be further optimized and parallelized.

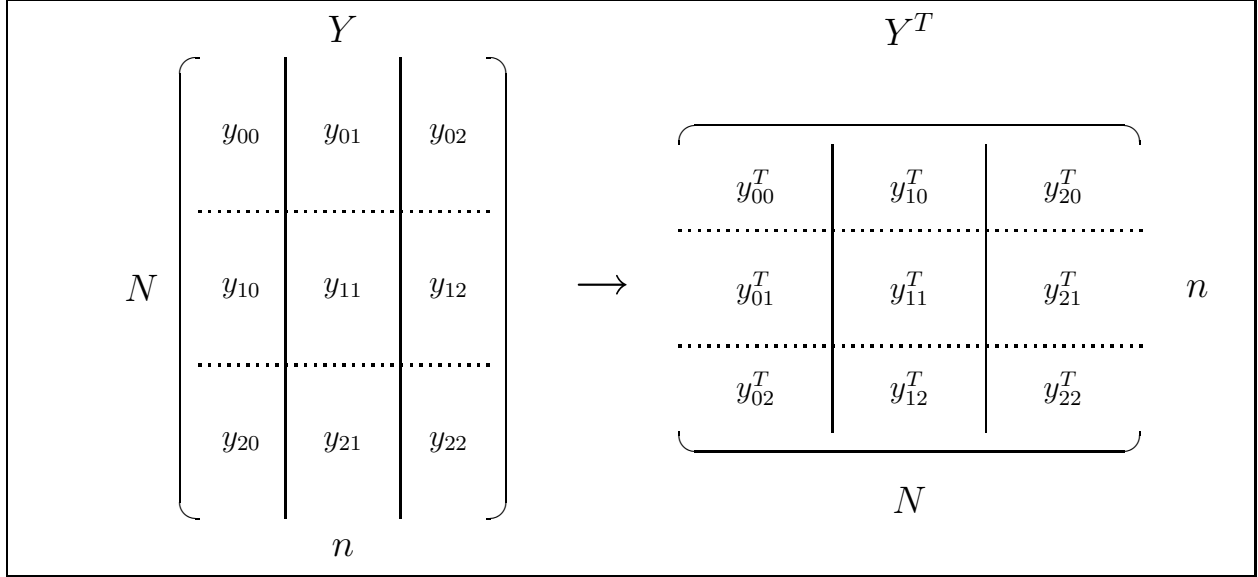


Figure 12: Transposition of distributed matrices – Schematic diagram showing how the transpose Y^T of the distributed `column_bundle` Y is obtained in a DMP calculation, which in this example has $p = 3$ processors. Across all the processors, Y is $N \times n$ and Y^T is $n \times N$. Solid vertical lines show the distribution of the columns of Y or Y^T among the processors, so that each processor stores a $N \times (n/p)$ block of Y and a $n \times (N/p)$ block of Y^T . The horizontal dotted lines show the division of Y and Y^T into blocks that must be communicated between processors to achieve the transposition: the block y_{ij} is sent from processor j to processor i . Processor i then transposes the block and stores it in the j th section of Y^T .

7.4.2 Distributed-memory (DMP) architectures

Parallelization on DMP architectures requires careful thought regarding how the memory distribution and inter-process communications are to be implemented. The most memory-consuming computational objects are the `column_bundles`, and for a large system, no single processor in a DMP computer can store the entire data structure in its local memory banks. Therefore, we parallelize the storage of `column_bundles` by distributing equal numbers of the columns comprising a `column_bundle` among the processors.

Given this distribution by columns, the application of basis-dependent operators is unchanged from how it is done in a serial context: each processor applies the operator to the columns that are assigned to it, and perfect parallelization is achieved as no inter-processor communication is required. The large basis-independent matrix products, however, are more challenging to parallelize as they necessarily involve inter-processor communication.

Consider again the product $M = Y_1^\dagger Y_2$, which in terms of components is given by

$$M_{ij} = \sum_k (Y_1)_{ki}^* (Y_2)_{kj}.$$

The column-wise parallel distribution of Y_1 and Y_2 means that the full range of the i and j indices is distributed among the processors while the full range of the k index is accessible locally by each processor. Since Y_1 and Y_2 are $N \times n$, each processor has a $N \times (n/p)$ block

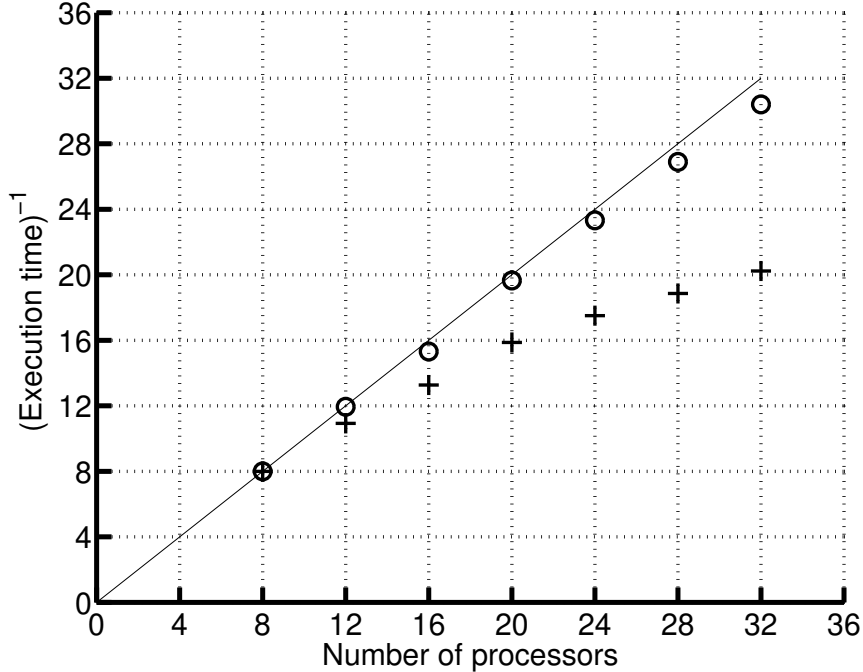


Figure 13: Scaling of DMP parallelization – Performance of the DMP parallelized plane-wave code for a 256 silicon atom system as a function of the number of processors for the parallelized $M = Y_1^\dagger Y_2$ multiplication (circles) and for the code overall (pluses). In both cases, the performance has been normalized to the respective performance with a single processor based on extrapolation from the eight processor run. The straight line with slope of unity represents ideal scaling for perfect parallelization.

(i.e. n/p columns of length N) in its local memory, where p is the number of processors. Unfortunately, computing M using this column-wise distribution requires a great deal of inter-processor communication. For example, the processor computing the i th row of M requires knowledge of *all* the columns of Y_2 , so that in total, the Nn data items describing Y_2 will have to be sent $p - 1$ times between all the processors.

A more efficient communication pattern can be developed that avoids this redundancy. Denoting the transpose of Y by Y^T , the matrix product can be rewritten as

$$M_{ij} = \sum_k (Y_1^T)_{ik}^* (Y_2^T)_{jk}.$$

Hence, if we first transpose Y_1 and Y_2 , then the column-wise distribution of the transposed `column_bundles` insures that the full range of the i and j indices can be accessed locally on each processor while the full range of the k index is now distributed among the processors. Figure 12 presents a schematic of how the transposition of a `column_bundle` Y is accomplished: each processor has a $N \times (n/p)$ block of Y whose contents it sends to $p - 1$ other processors as $p - 1$ blocks of size $(N/p) \times (n/p)$. Next, each processor receives $p - 1$ similar blocks sent to it by other processors, transposes them, and stores them in the appropriate sections of Y^T . Each processor sends or receives only $Nn(p - 1)/p^2$ data items, and a total of $Nn(p - 1)/p$ data items are communicated among all the processors.

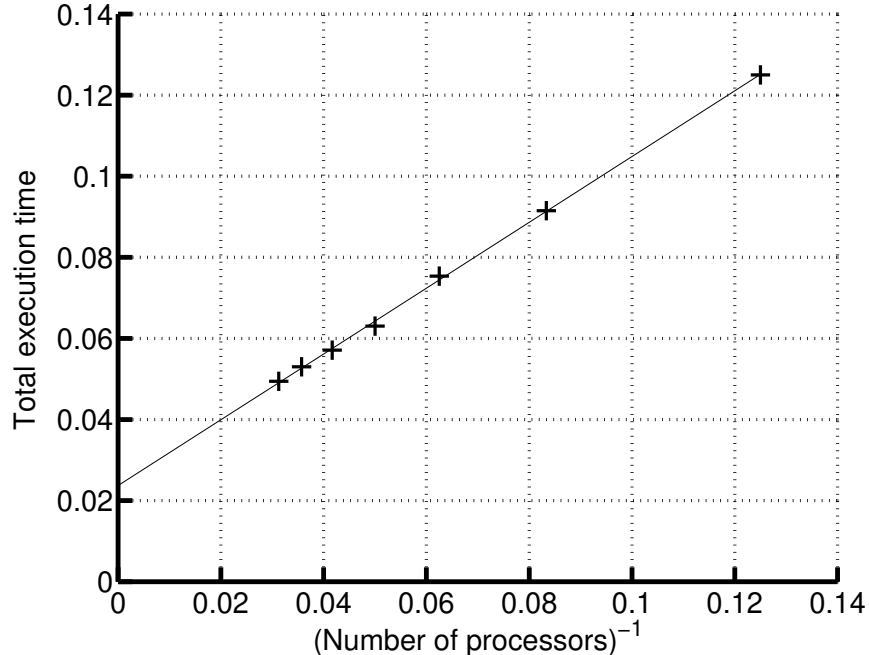


Figure 14: Amdahl’s analysis of DMP scaling – Total execution time of the DMP parallelized plane wave code for a 256 silicon atom system as a function of the reciprocal of the number of processors utilized. The line of least-squares fit to the data points is shown as well. Execution times are normalized in units of the execution time for a single processor as extrapolated based on the eight processor run.

The computation of M in the transposed mode has the same operation count as in the non-transpose mode (i.e. $O(n^2N)$ operations), which when distributed across processors, amounts to $O(n^2N/p)$ operations per processor. Of course, we block the matrix multiplications on each processor to ensure the best performance. Finally, a global sum across all the processors’ $n \times n$ resulting matrices is required to obtain the final answer M , and this requires $\log_2 p$ communications of size n^2 when using a binary tree.

Assuming that processors can simultaneously send and receive data across the network, the time required to perform the transpose is $O(nN/p)$, the time needed to perform the multiplications is $O(n^2N/p)$, and the time required to perform the final global sum is $O(n^2 \log_2 p)$. For large problem sizes, the time needed to perform the multiplications will always be larger than the time required for the communications by a factor of $\sim n$. Thus interprocessor communications are, in the end, never an issue for a sufficiently large physical system, and the computation will be perfectly parallelized in the asymptotic limit of an infinitely large system.

Figure 13 shows a plot of the performance of our DMP parallelized plane-wave code for a single conjugate-gradient step when run on a 256 atom silicon cell. The choice of pseudopotential, cutoff, and k -point sampling are the same as for the SMP calculation above. The basis set is of size $N = 23563$ and the system has $n = 512$ valence bands. The calculations were run on an IBM SP2 system with 336 nodes, and each node has four 332 MHz Power2 Architecture RISC System/6000 processors and 1.536 GB of memory. Again, we

see excellent and near perfect scaling for the parallelized matrix multiplications, validating our claim that the transposition approach combined with the large system size provides for very good parallelization. With 32 processors, each parallelized multiplication runs at an average rate of 188 MFLOPS per processor (57% of the processor clock rate), which is impressive given the fact that the processors are busily communicating the data required for the transpositions and global sums.

The plot also shows the saturation of the total performance of the code with increasing number of processors. With eight processors, the overall performance translates into an average rate of 254 MFLOPS per processor (76% of the clock rate), whereas with 32 processors the rate has reduced to 160 MFLOPS per processor (48% of the clock rate). Clearly, the serial portions of the calculation begin to contribute significantly to the run time of the code. Following the discussion of the SMP results above, Figure 14 presents a plot of the total execution time versus inverse number of processors. The extrapolated serial time T_0 in this case is only 2-3% of the total theoretical run time on a single processor, which shows how effectively the calculation has been parallelized. In addition, for the 32 processor run, the total run time is only two times larger than T_0 , signalling the end of significant gains from the use of more processors.

8 Acknowledgements

We would like to thank Jason A. Cline for his work in implementing the LSDA functional. We are immensely grateful to Tairan Wang for his work in creating the MPI implementation of the software and to Kenneth P. Essler for creating the MPI distributed transposition routine and the accompanying efficient matrix multiplication routines.

This work was supported primarily by the MRSEC Program of the National Science Foundation under award number DMR 94-00334, by the Alfred P. Sloan Foundation (BR-3456), and also by an ASCI ASAP Level 2 grant (contract numbers #B338297 and #B347887). Code development was carried out on the MIT Xolas prototype SMP cluster as well as on the MIT Pleiades Alpha cluster. The calculations were carried out on the Xolas cluster and on the ASCI Blue Pacific Teraflops IBM SP2 platform. This work made use of the Cornell Center for Materials Research Shared Experimental Facilities, supported through the NSF MRSEC program (DMR-9632275).

A Plane-wave implementation of the basis-dependent operators

A widely used basis-set for *ab initio* calculation has been the plane-wave basis set [7]. Plane waves are ideally suited for periodic calculations that model the bulk of a crystalline material. In addition, plane waves provide uniform spatial resolution throughout the entire simulation cell, and the results of the calculations can be converged easily by simply increasing the number of plane waves in the basis set. We will use plane waves as a concrete example of how the basis-dependent operators of Section 4.1 are to be implemented.

Given the lattice vectors of a periodic supercell, we compute the reciprocal lattice vectors and denote the points of the reciprocal lattice by the vectors $\{G\}$. Each element of our basis set $\{b_\alpha(r)\}$ will be a plane wave with vector G_α ,

$$b_\alpha(r) = \frac{e^{iG_\alpha \cdot r}}{\sqrt{\Omega}},$$

where Ω is the real-space volume of the periodic cell. This basis is orthonormal, and the overlap operator \mathcal{O} is the identity operator,

$$\mathcal{O} = I.$$

The integrals of the basis functions s are given by

$$s_\alpha = \sqrt{\Omega} \delta_{G_\alpha, 0},$$

so that the $\bar{\mathcal{O}}$ operator is given by

$$\bar{\mathcal{O}}_{\alpha\beta} = \delta_{\alpha,\beta} - \delta_{G_\alpha, 0} \cdot \delta_{G_\beta, 0}.$$

The Laplacian operator L is diagonal in this basis and is given by

$$L_{\alpha\beta} = -\|G_\alpha\|^2 \delta_{\alpha\beta}.$$

The forward transform \mathcal{I} is given by a Fourier transformation. Specifically, for a point p on the real-space grid, we have that

$$\mathcal{I}_{p\alpha} = \frac{e^{iG_\alpha \cdot p}}{\sqrt{\Omega}}.$$

Consider applying \mathcal{I} to the column vector χ and evaluating the result at the point p :

$$(\mathcal{I}\chi)_p = \sum_\alpha \mathcal{I}_{p\alpha} \chi_\alpha = \frac{1}{\sqrt{\Omega}} \sum_\alpha e^{iG_\alpha \cdot p} \chi_\alpha.$$

This is the forward Fourier transform of χ .

For the case of plane waves, the inverse transform \mathcal{J} can be chosen to be the inverse of \mathcal{I} , $\mathcal{J} = \mathcal{I}^{-1}$, as per the discussion of Section 4.1. It follows that

$$\mathcal{J} = \mathcal{I}^{-1} = \left(\frac{\Omega}{N}\right) \mathcal{I}^\dagger \quad \text{or} \quad \mathcal{J}_{\alpha p} = \frac{\sqrt{\Omega}}{N} e^{-iG_\alpha \cdot p},$$

where N is the number of points in the real-space grid. Applying \mathcal{J} to a column vector ξ , we have

$$(\mathcal{J}\xi)_\alpha = \frac{\sqrt{\Omega}}{N} \sum_p e^{-iG_\alpha \cdot p} \xi_p.$$

Thus \mathcal{J} is a reverse Fourier transform. The operators \mathcal{I}^\dagger and \mathcal{J}^\dagger are also Fourier transforms with appropriate scaling factors. Computationally, Fast Fourier Transforms [3, 21] can be used to implement these operators most efficiently.

The last remaining basis-dependent item is the ionic potential V_{ion} . For periodic systems, this potential is a periodic sum of atomic potentials $V_{at}(r)$,

$$V_{ion}(r) = \sum_{R,I} V_{at}(r - R - r_I),$$

where R ranges over the real-space lattice sites, I ranges over the atoms in the unit cell, and r_I is the position of the I th atom. Based on this, the elements of the vector V_{ion} of Eq. (13) are given by

$$(V_{ion})_\alpha = \frac{S(G_\alpha) \hat{V}_{at}(G_\alpha)}{\sqrt{\Omega}},$$

where the structure factor $S(q)$ is given by

$$S(q) \equiv \sum_I e^{-iq \cdot r_I},$$

and the Fourier transform of the atomic potential \hat{V}_{at} is defined by

$$\hat{V}_{at}(q) \equiv \int d^3r e^{-iq \cdot r} V_{at}(r).$$

B Non-local potentials

In this section we show how non-local potentials can easily be incorporated into the DFT++ formalism. The total non-local potential operator \hat{V} for a system is given by a sum over each atom's potential,

$$\hat{V} = \sum_I \hat{V}_I,$$

where \hat{V}_I is the non-local potential of the I th atom. The non-local energy is given by the expectation of \hat{V} over all the occupied states $\{\psi_i\}$ with fillings f_i ,

$$E_{nl} = \sum_i f_i \langle \psi_i | \hat{V} | \psi_i \rangle = \sum_I \sum_i f_i \langle \psi_i | \hat{V}_I | \psi_i \rangle.$$

Given the linearity of E_{nl} with respect to the atoms I , in our discussion below we will only consider the case of a single atom and will drop the index I . The results below can then be summed over the atoms to provide general expressions for multiple atoms.

Using the expansion coefficients $C_{\alpha i}$ of Eq. (7), we rewrite the non-local energy as

$$E_{nl} = \sum_i f_i \langle \psi_i | \hat{V} | \psi_i \rangle = \sum_{i,\alpha,\beta} f_i C_{\alpha i}^* \langle \alpha | \hat{V} | \beta \rangle C_{\beta i} = \text{Tr}(VCF C^\dagger) = \text{Tr}(VP), \quad (45)$$

where $|\alpha\rangle$ is the ket representing the basis function $b_\alpha(r)$, P is the single-particle density matrix of Eq. (20), the matrix F was defined as $F_{ij} = \delta_{ij}f_i$, and the matrix elements of the non-local potential are defined as

$$V_{\alpha\beta} \equiv \langle \alpha | \hat{V} | \beta \rangle = \int d^3r \int d^3r' b_\alpha^*(r) V(r, r') b_\beta(r').$$

The matrix V clearly depends on both the basis set and the potential. The contribution of the non-local potential to the total Lagrangian of Eq. (29) is given simply by $\text{Tr}(VP)$. Following the derivations of Eqs. (35) and (36), we see that the single-particle Hamiltonian H is modified only by the addition of V ,

$$H = -\frac{1}{2}L + \mathcal{I}^\dagger [\text{Diag } V_{sp}] \mathcal{I} + V. \quad (46)$$

We now write the potentials in separable form,

$$\hat{V} = \sum_{s,s'} |s\rangle M_{ss'} \langle s'|, \quad (47)$$

where s and s' range over the quantum states of the atom, $M_{ss'}$ are matrix elements specifying the details of the potential, and $|s\rangle$ is the ket describing the contribution of the s th quantum state to the potential. Typical choices of s are the traditional atomic state labels nlm and possibly the spin σ . Once we define the matrix elements $K_{\alpha s} \equiv \langle \alpha | s \rangle$, which are again basis-dependent, we find two equivalent forms for E_{nl} ,

$$\begin{aligned} E_{nl} &= \sum_{i,s,s'} f_i \langle \psi_i | s \rangle M_{ss'} \langle s' | \psi_i \rangle = \sum_{i,s,s',\alpha,\beta} f_i C_{\alpha i}^* K_{\alpha s} M_{ss'} K_{\beta s'}^* C_{\beta i} \\ &= \text{Tr} \left[M (K^\dagger C) F (K^\dagger C)^\dagger \right] = \text{Tr} \left[K M K^\dagger P \right]. \end{aligned} \quad (48)$$

The first form involving $K^\dagger C$ is most useful for efficient computation of the energy, and the second form is most useful for derivation of the gradient (cf. the discussion of Eqs. (28) and (29)). The energetic contribution to the Lagrangian is given by Eq. (48) and the contribution to the Hamiltonian H is $K M K^\dagger$, which replaces V in Eqs. (45) and (46).

A further specialization involves the popular case of Kleinmann-Bylander potentials [20] where the double sum in Eq. (47) is reduced to a single sum over s . Thus, the matrix M is diagonal with elements m_s . The expression for the total non-local energy, this time including the sum over atoms I , is

$$E_{nl} = \sum_{I,s} m_{I_s} (K_{I_s}^\dagger C) F (K_{I_s}^\dagger C)^\dagger = \text{Tr} \left[\left(\sum_{I,s} m_{I_s} K_{I_s} K_{I_s}^\dagger \right) P \right].$$

Unfortunately, this expression is not very efficient for evaluating the energy of a system with many atoms, as the sum on I is large but the matrix $K_{I_s}^\dagger C$ only has a single row. This limits our ability to exploit the cache effectively (which only occurs for large matrix sizes).

We can rewrite the above energy expression so as to employ larger matrices and thus achieve greater computational efficiency. To do this, we define a diagonal matrix \bar{M}_s that contains the m_{I_s} values for all the atoms, $(\bar{M}_s)_{IJ} \equiv \delta_{IJ} m_{I_s}$, and we define the matrices A_s via $(A_s)_{\alpha I} \equiv K_{I_s, \alpha}$. We then reorganize the previous expression for the non-local energy,

$$E_{nl} = \sum_s \text{Tr} \left[\bar{M}_s (A_s^\dagger C) F (A_s^\dagger C)^\dagger \right] = \text{Tr} \left[\left(\sum_s A_s \bar{M}_s A_s^\dagger \right) P \right].$$

If we have N basis functions, n quantum states $\{\psi_i\}$, and n_a atoms in the system, then C is $N \times n$ and A_s is $N \times n_a$. Thus, for large system sizes, the products $A_s^\dagger C$ involve matrices with large dimensions, and optimized matrix-multiplication routines function at peak efficiency.

C Multiple k -points

We consider the generalization of our formalism to the case of multiple k -points, which arises in the study of periodic systems. In periodic cells, the wave functions satisfy Bloch's theorem and can be labeled by a quantum number k , a vector in the first Brillouin zone. The quantum states obey the Bloch condition

$$\psi_k(r + R) = e^{ik \cdot R} \psi_k(r),$$

where R is a lattice vector of the periodic cell. This implies that $\psi_k(r) = e^{ik \cdot r} u_k(r)$ where u_k is a periodic function of r , $u_k(r + R) = u_k(r)$. We define the expansion coefficients C_k for the vector k as being those of the periodic function $u_k(r)$ and arrive at (cf. Eq. (7))

$$\psi_{km}(r) = e^{ik \cdot r} \sum_{\alpha} (C_k)_{\alpha m} b_{\alpha}(r), \quad (49)$$

where the integer m labels the energy bands (i.e. different states at the same value of k). The Fermi-Dirac fillings may also have a k -dependence and are denoted as f_{km} .

In addition to k -vectors, calculations in periodic systems attach a weight w_k to the wave vector k . The rationale is that we require the integrals of physical functions over the Brillouin zone in order to compute the Lagrangian, energies, and other quantities. Ideally, we would like to integrate a function $g(k)$ over the Brillouin zone, but in a practical computation this must be replaced by a discrete sum over a finite number of k -points with weights w_k . That is, we perform the following replacement

$$\int d^3k g(k) \rightarrow \sum_k w_k g(k).$$

The required generalizations of the DFT++ formalism are straightforward and are outlined below. The density matrices (cf. Eq. (20)) now depend on k -points

$$P_k = w_k C_k F_k C_k^\dagger,$$

where the filling matrix is $(F_k)_{mm'} = \delta_{m,m'} f_{km}$, and the expansion coefficient matrices C_k are given by Eq. (49). We define the total density matrix P through

$$P = \sum_k P_k.$$

The electron density n (cf. Eq. (21)) is given by

$$n = \sum_k \text{diag}(\mathcal{I} P_k \mathcal{I}^\dagger).$$

The electron-ion, exchange-correlation, and electron-Hartree energies depend only on n , and provided the above k -dependent expression for n is used, these contributions require no further modification from the forms already given in Eqs. (23), (24), and (27) respectively.

The only change required to the basis-dependent operators involves the use of the Laplacian for computing the kinetic energy. The proper generalization is to define k -dependent Laplacian matrices L_k through

$$(L_k)_{\alpha\beta} \equiv \int d^3r \left[e^{ik \cdot r} b_\alpha(r) \right]^* \nabla^2 \left[e^{ik \cdot r} b_\beta(r) \right].$$

This immediately leads to the following expression for the kinetic energy:

$$T = -\frac{1}{2} \sum_k \text{Tr} (L_k P_k).$$

We still require the operator L as defined in Eq. (9) for operations involving the Hartree field ϕ and the Poisson equation. The L operator is L_k evaluated at $k = 0$.

The generalization of non-local potentials (Appendix B) to multiple k -points is also straightforward. The energy expression of Eq. (45) generalizes to

$$E_{nl} = \sum_k \text{Tr}(V P_k).$$

Having completed the specification of the Lagrangian with multiple k -points, the generalizations required for the orthonormality condition and the expressions for the derivatives of the Lagrangian follow immediately. We introduce overlap matrices U_k and unconstrained variables Y_k (cf. Eqs. (31) and (33)),

$$U_k = Y_k^\dagger \mathcal{O} Y_k \quad \text{and} \quad C_k = Y_k U_k^{-1/2},$$

where for simplicity we have set all subspace-rotation matrices to identity, $V_k = I$. The differential of the Lagrangian takes the form (cf. Eq. (35))

$$d\mathcal{L}_{LDA} = \sum_k \text{Tr}(H_k dP_k).$$

The single-particle Hamiltonians H_k depend on k only through the kinetic operators L_k ,

$$H_k = -\frac{1}{2} L_k + \mathcal{I}^\dagger [\text{Diag } V_{sp}] \mathcal{I} + V.$$

The expression for the single-particle potential V_{sp} is unmodified from that of Eq. (36) as it only depends on the total electron density n . The term V is to be added only if non-local potentials are employed (see Appendix B).

The expressions of Eq. (37) for the derivative of the Lagrangian also generalize in the following straightforward way,

$$\begin{aligned} d\mathcal{L}_{LDA} &= 2 \text{Re} \sum_k \text{Tr} \left[dY_k^\dagger \left(\frac{\partial \mathcal{L}_{LDA}}{\partial Y_k^\dagger} \right) \right], \quad \text{where} \\ \left(\frac{\partial \mathcal{L}_{LDA}}{\partial Y_k^\dagger} \right) &\equiv w_k \left\{ \left(I - \mathcal{O} C_k C_k^\dagger \right) H_k C_k F_k U_k^{-1/2} + \mathcal{O} C_k Q_k ([\tilde{H}_k, F_k]) \right\}, \quad \text{and} \\ \tilde{H}_k &\equiv C_k^\dagger H_k C_k, \end{aligned}$$

where Q_k is the natural generalization of the Q operator which uses the eigenvalues and eigenvectors of U_k (Appendix E).

D Complete LDA code with k -points and non-local potentials

In this section, we summarize and gather together the expressions for the LDA Lagrangian and its derivatives in the DFT++ formalism for a system with k -points and non-local potentials. This type of system provides the natural starting point for studying bulk systems and the properties of defects in bulk-like systems [7].

As we have emphasized previously, it is sufficient for us to display the formulae for the Lagrangian and its derivatives because formulae in the DFT++ language specify all the operations that must be performed and translate directly into computer code. (See Section 7.) Given the Lagrangian and its derivatives, we can use a variety of methods to achieve self-consistency. (See Section 6.)

We follow the notation of Appendix C and refer the reader to it for relevant details and definitions. The point we wish to emphasize is the compactness of the formalism and how it allows us to specify an entire quantum-mechanical Lagrangian or energy function in a few lines of algebra which explicitly show the operations required for the computation. We specialize to the case of Kleinmann-Bylander [20] non-local potentials (Appendix B).

$$\begin{aligned}
 \mathcal{L}_{LDA} &= -\frac{1}{2} \sum_k w_k \text{Tr} (F_k C_k^\dagger L_k C_k) + (\mathcal{J}n)^\dagger [V_{ion} + \mathcal{O}\mathcal{J}\epsilon_{xc}(n) - \bar{\mathcal{O}}\phi] \\
 &\quad + \sum_k w_k \sum_s \text{Tr} (\bar{M}_s (A_s^\dagger C_k) F_k (A_s^\dagger C_k)^\dagger) + \frac{1}{8\pi} \phi^\dagger L\phi, \\
 \frac{\partial \mathcal{L}_{LDA}}{\partial Y_k^\dagger} &= w_k \left\{ (I - \mathcal{O}C_k C_k^\dagger) H_k C_k F_k U_k^{-1/2} + \mathcal{O}C_k Q_k ([C_k^\dagger H_k C_k, F_k]) \right\}, \\
 \frac{\partial \mathcal{L}_{LDA}}{\partial \phi^\dagger} &= -\frac{1}{2} \bar{\mathcal{O}}\mathcal{J}n + \frac{1}{8\pi} L\phi, \\
 H_k &= -\frac{1}{2} L_k + \mathcal{I}^\dagger [\text{Diag } V_{sp}] \mathcal{I} + \sum_s A_s \bar{M}_s A_s^\dagger, \\
 V_{sp} &= \mathcal{J}^\dagger V_{ion} + \mathcal{J}^\dagger \mathcal{O}\mathcal{J}\epsilon_{xc}(n) + [\text{Diag } \epsilon'_{xc}(n)] \mathcal{J}^\dagger \mathcal{O}\mathcal{J}n - \mathcal{J}^\dagger \bar{\mathcal{O}}\phi.
 \end{aligned}$$

E The Q operator

In this appendix, we define the Q operator which appears in expressions for the derivative of the Lagrangian, e.g. in Eq. (37). The formal properties satisfied by Q are also presented, properties used in the derivation of the expression for the derivative based on the connection between Q and the differential of the matrix $U^{1/2}$. (See the derivation starting from Eq. (36) and resulting in Eq. (37) in Section 4.5.1.)

We start with the Hermitian matrix U . Let μ be a diagonal matrix with the eigenvalues of U on its diagonal, and let W be the unitary matrix of eigenvectors of U . Thus, the following relations hold: $U = W\mu W^\dagger$, $W^\dagger W = WW^\dagger = I$, and $UW = W\mu$.

Consider the differential of the matrix U . The Leibniz rule results in

$$dU = dW\mu W^\dagger + W d\mu W^\dagger + W\mu dW^\dagger.$$

Using the unitarity of W , we have

$$W^\dagger dUW = W^\dagger dW\mu + \mu dW^\dagger W + d\mu.$$

Differentiating the relation $W^\dagger W = I$, we have that $dW^\dagger W + W^\dagger dW = 0$ or $dW^\dagger W = -W^\dagger dW$. Substituting this above, we arrive at the relation

$$W^\dagger dUW = [W^\dagger dW, \mu] + d\mu. \quad (50)$$

This equation describes how differentials of the eigenvalues and eigenvectors of U are related to the differential of U , and it is simply a convenient matrix-based expression of the results of first-order perturbation theory familiar from elementary quantum mechanics. To see this equivalence, we first examine the diagonal elements of Eq. (50) and find

$$d\mu_n = (W^\dagger dUW)_{nn}, \quad (51)$$

the familiar expression for the first order shift of the eigenvalue μ_n . Considering off diagonal matrix elements of Eq. (50) leads to

$$(W^\dagger dW)_{nm} = \frac{(W^\dagger dUW)_{nm}}{\mu_m - \mu_n} \quad \text{for } n \neq m, \quad (52)$$

which is the expression for the first order shift of the m th wave function projected on the n th unperturbed wave function.

Next, we consider $f(U)$, an arbitrary analytic function of U . Using the eigenbasis of U , we can write $f(U) = Wf(\mu)W^\dagger$ where by $f(\mu)$ we mean the diagonal matrix obtained by applying f to each diagonal entry of μ separately. Following the same logic as above, the differential of $f(U)$ satisfies

$$W^\dagger d[f(U)]W = [W^\dagger dW, f(\mu)] + f'(\mu)d\mu.$$

Computing matrix elements of the above equation and using Eqs. (51) and (52), we arrive at the general result

$$(W^\dagger d[f(U)]W)_{nm} = (W^\dagger dUW)_{nm} \cdot \begin{cases} f'(\mu_n) & \text{if } m = n \\ \left[\frac{f(\mu_m) - f(\mu_n)}{\mu_m - \mu_n} \right] & \text{if } m \neq n \end{cases}. \quad (53)$$

We now apply this result to the case where $f(U) = U^{1/2}$. This means that $f(\mu_n) = \sqrt{\mu_n}$ and that $f'(\mu_n) = 1/(2\sqrt{\mu_n})$ in Eq. (53). By employing the algebraic identity $(\sqrt{x} - \sqrt{y})/(x - y) = 1/(\sqrt{x} + \sqrt{y})$, we arrive at the expression

$$(W^\dagger d[U^{1/2}]W)_{nm} = \frac{(W^\dagger dUW)_{nm}}{\sqrt{\mu_n} + \sqrt{\mu_m}} = (W^\dagger Q(dU)W)_{nm}, \quad (54)$$

where we define the operator $Q(A)$ for an arbitrary matrix A to be

$$(W^\dagger Q(A)W)_{nm} \equiv \frac{(W^\dagger AW)_{nm}}{\sqrt{\mu_n} + \sqrt{\mu_m}}. \quad (55)$$

From this definition of Q , it is easy to prove that the following identities are satisfied for arbitrary matrices A and B and arbitrary power p :

$$\begin{aligned}
 Q(dU) &= d[U^{1/2}] \\
 \text{Tr}(Q(A)B) &= \text{Tr}(AQ(B)) \\
 \text{Tr}(Q(U^p A)B) &= \text{Tr}(U^p Q(A)B) \\
 \text{Tr}(Q(AU^p)B) &= \text{Tr}(Q(A)U^p B) \\
 A &= Q(A)U^{1/2} + U^{1/2}Q(A).
 \end{aligned}
 \tag{56}$$

These are the identities used in the derivation of the expression for the derivative of the Lagrangian with respect to Y in Section 4.5.1.

References

- [1] T.A. Arias, M.C. Payne, and J.D. Joannopoulos, *Physical Review Letters* **69**, 1077 (1992).
- [2] W. Kohn and L.J. Sham, *Physical Review* **140**, A1133 (1965).
- [3] M. Frigo and S.G. Johnson, "FFTW: An Adaptive Software Architecture for the FFT," Proc. ICASSP 1998, vol. 3, p. 1381. The software package is available at <http://www.fftw.org>
- [4] R. Lippert, T.A. Arias, and A. Edelman, *Journal of Computational Physics* **140** 270 (1998).
- [5] T.A. Arias, *Reviews of Modern Physics* **71** 267 (1999).
- [6] T.A. Arias and T.D. Engeness, "Beyond Wavelets: Exactness theorems and algorithms for physical calculations", Computer Simulation Studies in Condensed Matter Physics XII, Eds. D. Landau, S.P. Lewis, and H.B. Schuttler (Springer Verlag, Heidelberg, 1999).
- [7] M.C. Payne, M.P. Teter, D.C. Allan, T.A. Arias, and J.D. Joannopoulos, *Reviews of Modern Physics* **64**, 1045 (1992), and references therein.
- [8] For recent developments, see J.E. Whiteman, The Mathematics of Finite Elements and Applications: Highlights 1996 (John Wiley & Sons, New York, 1997); for an introduction, see T. Chandrupatha and A. Belegundu, Introduction to Finite Elements in Engineering (Prentice Hall, Upper Saddle River, NJ, 1997).
- [9] E.R. Davidson and D. Feller, *Chemical Review* **86** 681 (1986); S. Wilson, *Advances in Chemical Physics* **67** 439 (1987).
- [10] O. Gunnarson and B.I. Lundqvist, *Physical Review B*, **13**, 4274 (1976).
- [11] R.G. Parr and W. Yang, Density-Functional Theory of Atoms and Molecules (Oxford U. Press, New York, 1989).

- [12] J. Perdew and A. Zunger, *Physical Review B*, **23**, 5048 (1981).
- [13] S. Goedecker and C.J. Umrigar, *Physical Review A*, **55**, 1765 (1997).
- [14] X. Gonze, D.C. Allan, and M.P. Teter, *Physical Review Letters* **68** 3603 (1992).
- [15] D.D. Johnson, *Physical Review B* **38** 12807 (1988), and references therein.
- [16] P. Wesseling, An Introduction to Multigrid Methods (Wiley, Chichester, New York, 1992).
- [17] S. Obara and A. Saika, *Journal of Chemical Physics* **84** 3963 (1986).
- [18] W.H. Press, B.P. Flannery, S.A. Teukolsky, and W.T. Vetterling, Numerical Recipes in C, (Cambridge U., Cambridge, 1988).
- [19] N. Marzari, D. Vanderbilt, and M.C. Payne, *Physical Review Letters* **79**, 1337 (1997).
- [20] L. Kleinmann and D.M. Bylander, *Physical Review Letters* **48**, 1425 (1982).
- [21] J.W. Cooley and J.W. Tukey, *Mathematics of Computation* **19** 297 (1965); P. Duhamel and M. Vetterli, *Signal Processing* **19** 259 (1990).
- [22] G. Beylkin, R.R. Coifman, and V. Rokhlin, *Commun. Pure and Appl. Math.* **44** 141 (1992).
- [23] S. Ismail-Beigi and T.A. Arias, *Physical Review B* **57** 11923 (1998).
- [24] G. Csanyi, S. Ismail-Beigi, and T.A. Arias, *Physical Review Letters* **80** 3984 (1998).